Biotechnology Advances xxx (2016) xxx–xxx

Contents lists available at ScienceDirect

Biotechnology Advances

journal homepage: www.elsevier.com/locate/biotechadv

Point-of-Need bioanalytics based on planar optical interferometry

E. Makarona [a], P. Petrou [b], S. Kakabakos [b], K. Misiakos [a], I. Raptis [a,*]

[a] Optical Biosensors Lab, Institute of Nanoscience and Nanotechnology, NCSR "Demokritos", 15310 Athens, Greece
[b] Immunoassay/Immunosensors Lab, Institute of Nuclear & Radiological Sciences & Technology, Energy & Safety, NCSR "Demokritos", 15310 Athens, Greece

ARTICLE INFO

Article history:
Received 2 November 2015
Received in revised form 9 February 2016
Accepted 9 February 2016
Available online xxxx

Keywords:
Biosensor
Point-of-Need
Label-free detection
Planar waveguide
Interferometry
Biofunctionalization

ABSTRACT

This review brings about a comprehensive presentation of the research on interferometric transducers, which have emerged as extremely promising candidates for viable, truly-marketable solutions for PoN applications due to the attested performance that has reached down to 10^{-8} in term of effective refractive index changes. The review explores the operation of the various interferometric architectures along with their design, fabrication, and analytical performance aspects. The issues of biosensor functionalization and immobilization of receptors are also addressed. As a conclusion, the comparison among them is attempted in order to delve into and acknowledge their current limitations, and define the future trends.

1. Introduction — historical background

The 20th century was characterized as the era of information, where the means for acquiring, storing and distributing almost instantaneously information worldwide were developed and have since infiltrated our lives in ways that were unfathomable 50 years ago. A wide range of diverse methodologies and techniques have been developed at a staggering pace in order to enrich the "armory" of scientists in their pursuit to understand and more effectively fight and treat disease, discover new and more effective therapies for hard-to-treat or deadly conditions, achieve prognosis or early diagnosis of ailments even at the asymptomatic stage, effectively screen our food for harmful substances or even help keep the world safe against epidemics or bioterrorist threats. It is not by chance that the 21st century was named the era of biology since a large part of scientific endeavors aim at comprehending the biological pathways that ensure, determine and affect our well-being. In this intense effort, numerous scientists are trying to devise the next generation of biosensors capable not only of analyzing pertinent biological entities related to disease but also of helping in the discovery of new drugs, personalized treatment schemes, pre-cautionary food monitoring, environmental monitoring and safety and security systems. In the greater picture, these advances are to be combined with the "gifts" of the information era and to be communicated through a worldwide net that can set the basis for a better quality of life for every passenger on our blue dot in the cosmos.

The core element of these systems is the "biosensor", which as a word has had a quite large range of meanings. According to IUPAC definition, "A biosensor is a self-contained integrated device which is capable of providing specific quantitative or semi-quantitative analytical information using a biological recognition element (biochemical receptor) which is in direct spatial contact with a transducer element. A biosensor should be clearly distinguished from a bioanalytical system, which requires additional processing steps, such as reagent addition" (Koyun et al., 2012).

Thus a biosensor consists of two main parts, the specific biomolecule that interacts (binds or recognizes) with the analyte under study and the transducer (exploiting one among a wide range of transduction principles such as optical, piezoelectric, and electrochemical) that translates the output signal resulting from the biomolecular interaction to a signal that is easily measured (typically an electrical or optical signal).

The output signal from the transducer is recorded by an appropriate measuring apparatus that is equipped with all necessary interfaces to the transducer e.g., electrical, fluidic, optical ones. These measuring apparatuses are designed to match the particular needs of the particular transducer. In the most advanced applications the reader is an autonomous unit accommodating processing and optical presentation modules.

Even though the word "biosensor" is a relatively recent term, the principle of biosensing has been applied – unbeknownst as such at the time – hundreds of years ago: the canary in the coal mines is probably the oldest reported biosensor. However by considering the definition above, the first biosensor was introduced by Clark and Lyons who immobilized glucose oxidase (GOD) on an amperometric oxygen electrode surface semipermeable dialysis membrane in order to directly

* Corresponding author.
E-mail address: i.raptis@inn.demokritos.gr (I. Raptis).

http://dx.doi.org/10.1016/j.biotechadv.2016.02.005
0734-9750/

quantify glucose concentration in a sample. In their ground breaking article (Clark and Lyons, 1962) they presented "intelligent" electrochemical sensors (pH, polarographic, potentiometric or conductometric) by adding enzyme transducers as membrane-enclosed sandwiches. Soon enough, the importance of developing devices capable of detecting biological entities and the transformational impact they could bring about became apparent to the scientific community. Indicative is the trend of publications containing the word "biosensor" in their abstract: from 1 in the year 1980 to 57 in the year 1990 and 463 in the year 2000, and to 1735 in the year 2010 (source: www.scopus.com). During the same period, new journals were launched focusing on miniaturized microsystems capable of measuring markers related to human health and the quantitative determination of harmful species in food, water or environmental samples.

During the past decade, another demand has been induced to biosensors: apart from the race for lower limits of detection, higher resolution and dynamic range, multi-parameter analysis capabilities, cost- and time-effectiveness or even the degree of user-friendliness, biosensors are envisioned to break free from the laboratory settings and to become applicable for on-the-spot determinations that are to be transmitted in real-time through the "cloud". A new term was coined to describe the envisioned systems, that of "Point-of-Need", with applications extending to a wide range of diverse areas including human health, food safety, environmental monitoring, and forensics.

Due to the importance of biosensors per se, but also the ever increasing importance of portable biosensing systems and their envisioned applications, significant public and private funding opportunities have become available all over the world via either international or national schemes. Next to these, companies active in the area of analytical devices have started their own research activities trying to develop solutions with particular emphasis on portable and at-the-spot measuring systems addressing the demanding requirements of PoN determinations. Lately, several companies have attracted funding through crowd funding schemes with TellSpec and Consumer Physics raising ~400 K USD and ~2.8 M USD, respectively, for the development of miniaturized tools for the identification of harmful species in food at the Point-of-Need.

Among all the applications, Point-of-Care (PoC) diagnostics are expected to be the largest contributor to the overall biosensors market, holding ~57% share (Source: Markets and Markets survey: http://www.marketsandmarkets.com/Market-Reports/biosensors-market-798.html), since there is a strong need to reform the current healthcare infrastructure in the developed world so as to accommodate for an ever increasing aging population, and to contribute to the amelioration of the healthcare system in the developing parts of the globe. The key players in this industry include F. Hoffmann-La Roche Ltd. (Switzerland), LifeScan Inc. (U.S.), Bayer Healthcare AG (Germany), Abbott Point of Care Inc. (U.S.), Medtronic (U.S.), Siemens Healthcare (Germany), and others.

In addition, important prizes have been announced for the development of holistic solutions that have been able to measure the concentration of multiple analytes at the PoN, with the most recent ones to be:

a) The *Xprize Tricorder*, a 10 MUSD competition to develop a portable, wireless device in the palm of a hand that could monitor and diagnose over a dozen medical conditions (http://tricorder.xprize.org/), and
b) The *H2020 Food Scanner*, a 1 MEuro prize to develop an affordable and non-invasive mobile solution that will enable users to measure and analyze their food intake (http://ec.europa.eu/research/horizonprize/index.cfm?prize=food-scanner).

The intense and long research effort along with public and private funding led to significant technological developments that allowed tremendous progress regarding the development of reliable and miniaturized biosensors for various clinical and non-clinical applications. In order to address the PoN needs, the research effort on biosensors has been channeled in a wide range of diverse transduction principles and applications. Traditionally, biosensors are classified on the basis of the following:

a) The use or not of a label
b) The transduction principle and
c) The bio-recognition component.

Both labeled and label-free approaches are explored intensively and in parallel since each approach offers its own competitive advantages. The labeled methodologies are relying on either fluorescent or magnetic labels bound directly to reporter biomolecules (antibodies or analyte analogs). Labeled approaches have shown excellent performance in terms of the limit of detection (LOD), since the signal from the binding events is amplified by several orders of magnitude allowing thus the detection of ultralow concentrations of the analyte of interest. As a result of this substantial advantage, numerous platforms have been developed and some of them have reached their path to the bioanalytics market. However, labeling approaches present a set of disadvantages when compared to label-free ones, and thus the potential user should weigh them prior to the final decision on which route one should select for the biosensor development. First and foremost, labeling adds to the final analysis cost, since the labels themselves can be rather costly and have limited shelf lifetimes. Furthermore, despite the added benefit of signal amplification, incorporating the labels onto biomolecules may negatively affect their functionality with a clear impact on the detection sensitivity (Fan et al., 2008), as it has been reported by Sun et al. for the effect of labeling on antigen–antibody affinity reactions (Sun et al., 2008). Finally, the presence of labels molecules can have a direct effect on the surface occupancy by the targeted analytes rendering the quantitative analysis of surface coverage and hence the actual LODs expressed in surface coverage density (mass/area) complicated. Exactly due to the aforementioned limitations, significant effort is directed towards the design and implementation of non-labeled methodologies. The first reported label-free methodologies were inferior in terms of analytical performance when compared with the labeled ones; however the latest generations offer excellent results in terms of the LOD, sensitivity, resolution, and assay time.

When the classification is based on the transduction principle, the biosensors are categorized into electrochemical, optical, piezoelectric, and thermal ones with an electrochemical glucose oxidase (GOx) sensor to be the first one reported in the literature (Clark and Lyons, 1962). Interestingly, the particular biosensor is still the most widely used, despite the fact that significant improvements were introduced throughout the years. The wide use of the particular biosensor most probably is grounded on the following characteristics in terms of application and transduction principle: the concentration range of the particular analyte is high and thus easily measured, the particular transduction principle is simple and low-cost thanks to the fabrication technology employed, and the interface with conventional electronic circuits for operation and signal acquisition is rather straightforward and facile. However, in addition to the characteristics of this legendary biosensor, there are several issues that should be further addressed in order to allow the introduction of additional electrochemical biosensors into the market.

On the other hand, there are numerous classes of label-free biosensors, which are in essence based upon the determination of an inherent biomolecular physical property, most commonly the index of refraction or mass. The optical transducers appear to be the preferred ones over their counterparts relying on the detection of mass changes (e.g. QCM or microcantilevers), or electrochemical ones, a preference that is prevalent both in the research and market domains. For example, although electrochemical biosensors currently account for the largest market by technology, most probably due to the glucose

Please cite this article as: Makarona, E., et al., Point-of-Need bioanalytics based on planar optical interferometry, Biotechnol Adv (2016), http://dx.doi.org/10.1016/j.biotechadv.2016.02.005

biosensors, the market for optical biosensors is the fastest growing segment and is expected to grow at a CAGR of over 10% from 2012 to 2018 (Source: Markets and Markets survey: http://www.marketsandmarkets.com/Market-Reports/biosensors-market-798.html).

Photonic probing in microsystem based bioanalysis has certain advantages over competing approaches. Being a contactless method, it galvanically isolates the sensing element from the excitation and detection electronics and provides more degrees of freedom in the detection schemes (Turner, 2000; Fan and White, 2011; Monat et al., 2007). Thus, it is expected that portable interferometric devices will soon find their place as the core elements in Point-of-Need devices aiming to decentralized sensing (Preechaburana et al., 2012).

Historically, the first optical sensor appeared as early as in 1937, when Langmuir and Schaefer described the determination of a biomolecule adlayer thickness formed on a metallic surface via the observation of colors produced by reflective interference (Langmuir and Shaefer, 1937). Some thirty years later, the use of ellipsometry for the observation and measurement of molecules immunoadsorbed on a surface was demonstrated (Vroman and Adams, 1969). The true boom though of optical biosensors did not come until the mid-90s since they had to wait for the maturing of microfabrication technologies and detection systems. Since then, optical biosensors, and even more specifically label-free optical biosensors have become one of the most active and attractive sectors of the biosensors development arena.

The preference on optical label-free biosensors is mainly attributed to a number of unique characteristics such as:

a) The use of light, which rules out any electrical interference facilitating this way multi-analyte determinations,
b) The excellent bioanalytical performance in terms of the LOD and sensitivity,
c) The high-resolution capabilities and, the potential for a high dynamic range,
d) and most importantly in terms of developing compact PoN systems
e) Their fabrication with standard microelectronic/micromachining processes that guarantee cost-efficient mass production on existing facilities.

The superior bioanalytical performance of optical biosensors is achieved through the real-time monitoring of minute refractive index changes due to the binding of the target molecules on the bioreceptors immobilized onto the sensor surface. The fast signal acquisition and the use of very accurate and with high sensitivity optical modules allow for the detection of infinitesimally thin biomolecular adlayers causing minuscule changes of either the intensity of the output signal or the spectral content. In addition, the detection of more than one analyte is achieved through multiplexing of multiple biosensors densely integrated on the same substrate. Last but not least, the fabrication of the majority of optical label-free biosensors is performed with standard microelectronic/micromachining processes. This way the tremendous improvements of these technologies can be straightforward applied to optical biosensors improving their analytical performance, size, reproducibility, and cost. Moreover, thanks to the advances in the Si processing technologies, it is possible to fabricate at low-cost transducers that were difficult to be realized in high volumes with the technologies available in the past.

Finally, when the classification is based on the bio-recognition component then the biosensors are categorized as sensors employing antibodies, enzymes, nucleic acids, cell receptors and even whole cells. Apart from these "naturally occurring" biorecognition elements, synthetic molecules like peptide nucleic acids (PNA), aptamers, and molecularly imprinted polymers (MIP) have been also employed as recognition elements due to their ability to specifically capture target molecules from complex matrices.

1.1. Scope of the review

Needless to point out that it would not be a possible feat to describe all optical biosensors in a single review paper, even when narrowing them down to label-free ones. Therefore, this review has concentrated mainly on label-free integrated interferometric methods, since they exhibit one of the greatest potentials for viable, truly-marketable solutions for PoN applications. Integrated optical biosensors have been recognized even from the early 90s as one of the most elegant and powerful techniques for direct affinity sensing mostly because of their increased sensitivity in terms of adlayer formation detection combined with their "limited sensitivity" in terms of thermal fluctuations and buffer solution refractive index changes compared to SPR (Lukosz, 1991). In particular, interferometry has been proved capable of impressive LODs (10^{-6}–10^{-7} expressed in effective refraction index changes or a few pg/mm^2 if expressed as surface coverage) even without the use of labels.

The remaining of the article is divided into the following sections: Section 2 is devoted to the description of interferometric sensors, starting with the more "classical" approaches of single-wavelength Mach–Zehnder (SW-MZIs) and Young interferometers (YIs) moving on to the more recently reported multi-color or polychromatic interferometers, and ending with the heteromodal/bi-modal interferometers. Section 3 addresses the issues of biosensor functionalization and immobilization of biorecognition elements. In the final section (Section 4) an effort is done to compare the existing interferometric techniques and to discuss their current limitations while also providing an insight into the challenges that need to be overcome and the emerging trends that need to be met for rendering label-free interferometers into marketable PoN systems.

In Table 1 the historical progression of the optical biosensors field is listed, taking into account certain breakthroughs.

2. Integrated optical interferometric sensors

2.1. Introduction to integrated optical sensors

As already mentioned in the introduction, the need to understand the biological mechanisms behind the functions of living organisms has led researchers to explore various means and methods not only to observe but also to monitor and quantify pertinent bioreactions. As early as the mid-'30s and then the late '60s (Langmuir and Shaefer, 1937; Vroman and Adams, 1969) probing molecules with light emerged as a promising, non-destructive means to closely observe and measure biomolecules in real-time. Soon thereafter, and with the aid of the semiconductor and telecommunications industry, integrated optical (IO) sensors containing waveguides and optical circuitry – mostly in the form of planar waveguides – appeared as a powerful tool for biosensing schemes of high-sensitivity and selectivity detection in real-time, and with improved multiplexing detection capabilities. These IO sensors could be developed to cost-efficient solutions since they could be fabricated by standardized industrial methods. The first demonstration of an IO sensor detecting humidity variations was reported in 1983 by Lukosz and Tiefenthaler (Lukosz and Tiefenthaler, 1983) who monitored variations in the intensity of output light coupled to SiO_2–TiO_2 waveguides when they exhaled towards or holding a finger near them.

The basic principle behind the operation of IO sensors is conceptually simple and applies to all IO sensors: the occurrence of a bioreaction or another biological entity (e.g., an adhered cell) on a part of the optical sensor (sensing region) influences either directly or via a chemo-optical transduction layer the propagation properties of a guided light beam travelling through the sensor. These changes in the propagation properties are directly translated into modulations of the optical output power recorded through external photodetectors and appropriate electronic modules. The modulations of

Please cite this article as: Makarona, E., et al., Point-of-Need bioanalytics based on planar optical interferometry, Biotechnol Adv (2016), http://dx.doi.org/10.1016/j.biotechadv.2016.02.005

Table 1
Historical progression of the field.

1	Langmuir and Shaefer (1937)	Determination of a biomolecule adlayer via the observation of colors produced by reflective interference
2	Clark and Lyons (1962)	First biosensor: glucose quantification by electrochemistry
3	Vroman and Adams (1969)	Measurement of molecules immunoadsorbed on a surface via ellipsometry
4	Lukosz and Tiefenthaler (1983)	The first demonstration of an IO sensor detecting humidity variations
5	Lukosz (1991)	Principles and sensitivities of integrated optical sensors for immunosensing were set.
6	Heideman et al. (1991)	Demonstration that slab Si_3N_4 waveguide with SiO_2 cladding layers is a promising bioanalytical device
7	Heideman et al. (1993)	Demonstration that planar MZI devices are able to detect effective refractive index changes in the 10^{-7} RIU regime
8	Brandenburg and Henninger (1994)	Young interferometer as optical sensor
9	Brandenburg (1997)	Young interferometry achieving the detection of refractive index changes in the 10^{-9} range
10	Ymeti et al. (2003)	Multiplexed operation of Young interferometry for multi-analyte detection
11	Luo et al. (2003)	First demonstration of broad-band Mach–Zehnder interferometry for the detection of hazardous organics
12	Misiakos et al. (2004)	The first monolithic silicon optoelectronic transducer for biosensing applications
13	Ymeti et al. (2005)	Young interferometry with standard Si processing process that has achieved the detection of effective refractive index changes in the 10^{-8} RIU range
14	Shew et al. (2008)	Polymeric interferometric devices implemented with standard microelectronic processing techniques
15	Kitsara et al. (2010)	Principle of operation of broad-band Mach–Zehnder interferometry for biosensing applications
16	Zinoviev et al. (2011)	Bi-modal interferometric sensors implemented with standard microelectronic/micromachining processes and significant results in terms of analytical performance
17	Mulder et al. (2012)	Design, implementation and evaluation of multiple wavelength Young interferometry
18	Misiakos et al. (2014b)	Monolithic implementation of broad-band Mach–Zehnder interferometry

the optical power can then be correlated to the biorecognition events. In most IO sensors, the changes of the optical parameters take place in the immediate vicinity of the core layers of the waveguides and are probed by the evanescent field of the propagating beam, which "senses" changes in the refractive index profile close to the sensor surface. As a result, most IO biosensors are called evanescent field biosensors and in several cases, the two terms are employed interchangeably. In general, the optical parameters that can be affected by the presence of a biorecognition event are the refractive index n, the absorption coefficient, and the luminescence, the latter should one opt for labeled techniques. Mathematically, these changes are expressed as changes in the complex phase velocity of the propagating beam, or more conveniently as changes of the complex effective index of refraction $\check{N} = N + iN^*$. Pure refractive index changes (refractometric sensors) modulate the real part of $\check{N}$, N, while absorption events in case of luminescent molecules (absorptive sensors) modulate the imaginary part N^*. In any case, the minimum detectable change of an IO sensor can be expressed as:

$$\Delta N_{min} = G(\lambda)\frac{\lambda}{L} \tag{1}$$

where λ is the vacuum wavelength of the propagating beam inside the IO sensor depending on the choice of the input source, L is the length (size) of the sensing region where the biorecognition binding events occur and affect the optical path of the propagating beam, and G(λ) is a "form factor" that is related to the design and nature of the sensor. In essence, the real part N of the effective refractive index of the guided modes becomes the most important physical quantity of a label-free IO sensor directly characterizing its analytical performance. ΔN_{min} depends on the wavelength λ of the input source, on the polarization of the input beam (TE or TM), the mode number m, and the properties of the waveguide itself, namely its geometrical characteristics and the refractive indices of its constituent layers. These parameters, even though they do not appear explicitly in Eq. (1) and are "contained" in the form factor G(λ), determine N as well as the penetration depth Δz of the evanescent field of the guided mode, which actually "probes" and "senses" the biomolecular reactions on the surface of the sensor. Δz is expressed as:

$$\Delta z = \frac{\lambda}{2\pi}\sqrt{N^2 - n_c^2} \tag{2}$$

where n_c is the refractive index of the covering medium over the sensing area.

Changes in the effective refractive index can be induced by two different effects that can take place separately or simultaneously (in most real-case applications both occur during a bioreaction):

- The formation of an adlayer of adsorbed or bound molecules on top of the sensing area having an effective thickness t_{ad} and an index of refraction n_{ad}
- Changes Δn_c in the refractive index n_c of the covering medium over the sensing area

Collectively, the induced effective refractive index changes can be described by

$$\delta N = \left(\frac{\partial N}{\partial t_{ad}}\right)t_{ad} + \left(\frac{\partial N}{\partial n_c}\right)\delta n_c = S_{ad}\cdot t_{ad} + S_c\cdot \delta n_c \tag{3}$$

It is through the derivatives in Eq. (3) that the above-mentioned waveguide characteristics affect the changes of the effective refractive index, and hence determine the analytical capabilities of an IO sensor rendering IO sensors into a versatile and flexible platform for highly-sensitive detection applications. In many cases, these derivatives have been used as the figures of merit describing the performance of an IO sensor; $S_c = {}^{\partial N}/_{\partial n_c}$ is employed as the sensitivity to pure refractometric changes, while $S_{ad} = {}^{\partial N}/_{\partial t_{ad}}$ is used to describe the sensitivity of the sensor in detecting the build-up of an adlayer at the interface between the waveguide and the cover medium. Even since the late '80s, it was shown (Tiefenthaler and Lukosz, 1989) that fine-tuning of the waveguide parameters for SiO_2–TiO_2 and Si_3N_4-based waveguides can lead to refractive index sensitivities ${}^{\partial N}/_{\partial n_c}$ directly translated to minimum detectable effective refractive index changes down to $\Delta N_{min} = 4\times10^{-6}$, and adlayer sensitivities ${}^{\partial N}/_{\partial t_{ad}}$ that can result into minimum detectable changes in adlayer effective thickness δt_{ad} in the order of 10 pm, or in other words to a fraction of a protein monolayer. Apart from S_c and S_{ad}, another parameter is encountered in literature as a figure of merit describing the performance of an IO sensor, in an effort to quantify the adsorbed molecules. This parameter is the so-called surface mass density Γ of the target molecule adlayer forming during the biorecognition reaction and is expressed as mass per unit area and calculated through De Feijter's formula (De Feijter et al., 1978):

$$\Gamma = t_{ad}\frac{n_{ad} - n_c}{{}^{\partial n_c}/_{\partial [c]}} \tag{4}$$

Please cite this article as: Makarona, E., et al., Point-of-Need bioanalytics based on planar optical interferometry, Biotechnol Adv (2016), http://dx.doi.org/10.1016/j.biotechadv.2016.02.005

where n_{ad} is the adlayer refractive index and $\partial n_c / \partial [c]$ is the derivative of the cover medium (in most cases a buffer solution) refractive index with respect to protein concentration. For most proteins $\partial n_c / \partial [c]$ is assumed to equal 0.0188 ml/g, since "the relation is based in the empirical result that the refractive index n_{ad} of protein solutions is linearly proportional to protein concentration [c], with the proportionality constant $\partial n_c / \partial [c]$ "(quoted from De Feijter et al. (1978)).

Γ is mentioned at this point, since later in this article an effort will be made to compare the state-of-the-art results, which are in general expressed in different figures of merit so as to allow their comparison to each other in a direct way.

In an effort to achieve and even surpass the theoretical limits of detection, several types of IO sensors have emerged during the last 20 years, and several reviews have already described the tremendous progress realized in this highly-paced field (Fan et al., 2008; Washburn and Bailey, 2011; Estevez et al., 2012; Kozma et al., 2014). Among these, the interferometric ones have emerged from the very beginning as extremely promising candidates not just because of their capability for highly sensitive *label-free* detection schemes, but also because of the fact that they can be realized via a large variety of materials most of which are employed and processed by microelectronic fabrication techniques or are based on commercial products. Compared to other IO sensors techniques, such as microring resonators, slot-waveguides, photonic crystals or even the commercialized SPRs, interferometric sensors are inherently donned with sensitivities in refractive index changes and adlayer formation of at least two orders of magnitude higher [see e.g. analysis in Lukosz (1991) or discussions in Washburn and Bailey (2011); Estevez et al. (2012)], do not have to compromise between dynamic range and resolution and can have a relatively long interaction length that can further push the analytical capabilities of the sensor (Eq. (1)).

The most commonly employed interferometric sensors are Mach–Zehnder (MZI) and Young interferometers (YI), while recently the principle of bi-modal interferometric sensors (Duval et al., 2012) has been applied with significant results in terms of analytical performance. In the next subsection, a short theoretical analysis of the "classical", single-wavelength (monochromatic) MZIs and YIs will be presented in order to conceptualize the inherent potential of these sensors for increased sensitivities. The analysis will be followed by an overview of various single-wavelength MZIs and YIs (hereafter referred to as SW-MZI and SW-YI) that have been realized and presented during the past 15 years, with some references dating a little earlier than that, from the '90s, not so much for historical reasons, but in order to demonstrate the inherent limitations and technological challenges of these two closely-related techniques, which have yet to be met and overcome. The second subsection is devoted to a more recent version of interferometry, which is based on multiple-wavelength or broad-band input sources, termed for simplicity in this paper as broad-band MZI (BB-MZI) and multi-wavelength YI (MW-YI). Again, a short theoretical analysis presenting the additional advantages of polychromatic interferometry compared to the more standard single-wavelength one precedes the presentation of recent publications on the subject. Finally, Section 2 is concluded with the description of other types of interferometric sensors following a similar format, namely, a short theoretical presentation and a summary of the recent advances.

2.2. Single-wavelength Mach–Zehnder and Young interferometry

2.2.1. Theoretical description of SW-MZI and SW-YI

In the dawn of the 19th century, Thomas Young, renowned polyglot, and physician of his time, in his presentation to the Royal Society (Young, 1802) described various interference phenomena, and soon after he performed his famous double-slit experiment (strictly speaking, a double hole experiment) (Young, 1804). In this experiment, a light beam was split through two slits. Because of the wave nature of light, each slit behaves as a point source and the two resulting wavefronts that now emanate from the tow separate sources, recombine and interfere in free space. When a screen is placed at a distance, a pattern of light and dark bands appear, called an interferogram. The width of the bands depends on the wavelength of light while their positioning depends directly on the difference in the optical paths of the two beams. Young's experiment could only be explained if one interpreted light as a wave, and thus the double-slit experiment played a vital part in the acceptance of the wave theory of light, vanquishing the corpuscular theory of light proposed by Isaac Newton.

Ninety years later, Ludwig Zehnder presented an apparatus capable of determining the relative phase shift variations between two collimated beams derived by splitting light from a single source (Zehnder, 1891). A year later, Zehnder's proposal was refined by Ludwig Mach, son of Ernst Mach (Mach, 1892) and we ended up with the well-known Mach–Zehnder Interferometer, a highly configurable instrument, in which in contrast to the much similar Michelson interferometer, each of the well-separated light paths is traversed only once.

The basic concept of both types of interferometry is to split a beam of light into two separate paths and then to allow them to recombine either through a new means of propagation (in the case of MZI) or in free space (in the case of YI). If the two paths have different optical properties, e.g. are made of a different material or a new material is inserted in one of the two paths, the two beams will travel at different velocities and when they recombine they will have a different phase. Due to the wave nature of light, the phase difference results in interference phenomena. Despite the fact that both interferometric techniques were devised in order to elucidate the nature of light and optical phenomena, it turned out that manipulating the light by splitting an input beam into two separate paths and then allowing them to recombine, can become a powerful tool for a variety of applications (for example, MZIs are routinely used in telecom applications) and more specifically as optical biosensors. Nearly two centuries after the efforts of Young to prove the wave nature of light, and one century after Mach and Zehnder's first demonstration of the interferometric apparatus, YIs and MZIs are turning into the heart of Point-of-Need systems that have the potential to radically transform the way disease is prognosed, diagnosed and treated, and how humanity can protect itself from epidemics or harmful substances several of which may be of its own devise.

In MZI, as shown in Fig. 1a, the initial beam is split into two arms which recombine again in a common path and interfere. In most cases the beam that is produced by the interference of the two beams is recorded by a photodetector. In essence, the output of an MZI device requires a light intensity measurement and it is through the modulations of that intensity that information is extracted about the material inserted over one of the arms. Due to the wave nature of light, the intensity I_{out} of the recorded light is mathematically expressed through:

$$I_{out} = \frac{I_{in}}{2}[1 + \cos(\Delta\phi(\lambda))] \tag{5}$$

where I_{in} is the input beam intensity and $\Delta\varphi(\lambda)$ is the phase difference between the two interferometric arms correlated to the effective refractive indices of the arms through:

$$\Delta\phi = \frac{2\pi L}{\lambda}[N_r(\lambda) - N_s(\lambda)] = \frac{2\pi L}{\lambda}\Delta N_{rs} \tag{6}$$

Eq. (5) is a periodic (sinusoidal) function of $\Delta\varphi$. When using a MZI as a biosensor, one of the arms (referred to as "sensing arm") is modified in such a way that it can capture targeted biomolecules from a sample one wishes to analyze. The other arm (referred to as "reference arm") is either covered and not in contact with the inserted sample or is chemically modified to be inert to molecules present in the sample. Any biorecognition binding event that can alter the effective refractive

Please cite this article as: Makarona, E., et al., Point-of-Need bioanalytics based on planar optical interferometry, Biotechnol Adv (2016), http://dx.doi.org/10.1016/j.biotechadv.2016.02.005

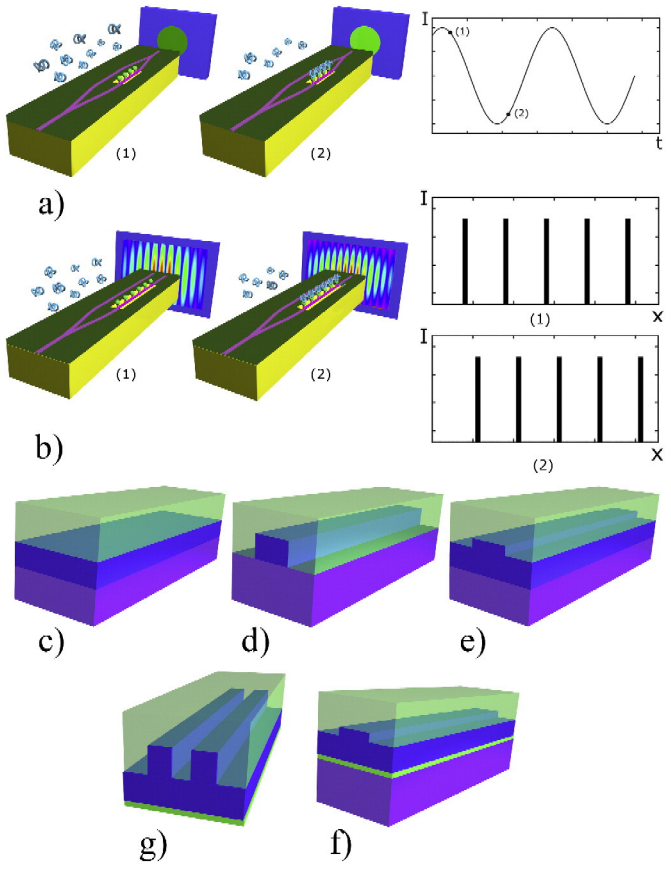

Fig. 1. Schematic representation of the principle of operation of (a) Mach–Zehnder interferometry, and (b) Young interferometry. In (a1) before the biorecognition event the output of the interferometer has an intensity I1 recorded in time. Upon binding of the analyte molecules over the appropriately functionalized sensing arm with specific probe molecules in (a2), the interference effect results in a sinusoidally modified intensity as shown in the graph on the right-hand side. In (b1), the analogous situation for the Young interferometer is shown: before binding of the analyte molecules the interference fringes are located in specific position over a detecting screen. Upon the biorecognition event the fringes shift to a new location (b2), as shown on the screen snapshots on the right-hand side of the figure. (c)–(g) Schematics of the most commonly employed waveguide structures in IO sensors (a) slab waveguides, (b) strip waveguides, (c) rib waveguides, (d) ARROW waveguides, and (e) slot waveguides.

index of the sensing arm by δN_s governed by Eq. (3), induces a new phase shift $\Delta\varphi' = 2\pi L\Delta N_s'/\lambda = 2\pi L[N_r - (N_s + \delta N_s)]/\lambda$ that modifies sinusoidally the output intensity according to Eq. (5) and shown schematically in Fig. 1a.

In the YI configuration (Fig. 1b), the two arms act as two closely spaced point sources in an analogy to Young's double-slit experiment. In an identical way to the MZI, one arm serves as the sensing element and is modified to capture targeted molecules through a biochemical reaction, and the other arm remains inert to the sample serving as a reference. The two output beams instead of recombining interfere in free space and form a pattern of alternating dark and bright fringes on the screen of a detector (most commonly a CCD camera), called interferogram. The intensity distribution along the detecting screen is given by the following equation

$$I(x,\lambda) = I_1 + I_2 + 2\sqrt{I_1 I_2}\cos\left[\frac{2\pi b}{\lambda D}\cdot x + \Delta\varphi(\lambda)\right] \quad (7)$$

where I_1, I_2 are the intensities of the two beams at the output, D is the distance of the sensor from the screen, and b is the distance between the two arms, Fig. 1b. $\Delta\varphi$ is given by the exact same equation applying to an MZI (Eq. (6)). In an analogous way, when a biorecognition binding event changes the effective refractive index of the sensing arm by δN_s, a new phase difference $\Delta\varphi$' between the two propagating beams will be induced. Then, instead of having an intensity variation recorded, the phase difference causes the fringes of the interferogram to move along the detection screen by a distance governed by Eq. (7). The change in the position of the interferogram is the quantity that is related to the biorecognition binding event and is correlated to the nature and concentration of the bound molecule.

In turning YIs and MZIs into integrated optical sensors, microfabrication techniques are exploited to construct the interferometers out of planar waveguides on rigid substrates, such as silicon or glass. The simplest scheme is to have an input waveguide where a polarized and monochromatic coherent beam is coupled into the sensor. The input waveguide is split into two arms – usually in the form of a Y-junction – which divides the input beam into two beams of equal power traveling through the two arms, as shown in Fig. 1a and b. One arm is used as a reference and the other acts as the sensing area. The biorecognition elements are to be bound on the specially functionalized sensing area and to be "probed" by the evanescent wave of the guided mode. The binding events that take place upon introduction of targeted analyte alter locally the effective index of refraction causing a phase lag between the two propagating beams. At the end of the sensing area the two beams (that have travelled with different velocities through the reference and sensing arms due to the binding events and have a phase difference between them) are either recombined through a common waveguide, and one obtains an MZI, or they are allowed to interfere in free space resulting into a YI the output of which can be detected as moving fringes on a screen placed at a distance from the waveguide outputs. The most fundamental prerequisite in order to transform a planar optical circuit into MZIs and YIs is that the waveguides support only one mode for the input source's wavelength. As briefly discussed in sub-section 2.1, the most important parameter in interferometric biosensing is the effective index of refraction over the sensing area, the variations of which due to a binding reaction are directly translated into intensity variations of the output light (in the case of MZI) or shifting fringes (in the case of YI). Should more than one mode exist within the waveguides for the same wavelength, the output signal would be scrambled since each propagating mode has a different effective index of refraction. There are several ways to fabricate single-mode (monomodal) waveguides, but such a description falls out of the scope of the present review and will not be elaborated further (the interested reader is referred to an excellent summary article by Kozma et al. (2014).

One very important parameter that is governing the sensitivity of the interferometric sensors is the length of the sensing area L. As seen in Eq. (6), the induced phase change is linearly proportional to L or expressed in a different way in Eq. (1), the minimum detectable effective refractive index change ΔN_{min} is inversely proportional to L. This attribute offers a competitive advantage to interferometric sensors which compared to other techniques may be designed in such a way as to increase the sensitivity through the size of the sensor itself. Nonetheless, L cannot be made arbitrarily long. First and foremost, increasing L increases the footprint of the entire sensor and even though cm-long interferometric sensors have been reported, having such large devices beats the purpose of miniaturization – a critical parameter for PoN applications – and increases the cost of fabrication (fewer sensors per processed wafer) with a direct impact on the final price of the PoN system. Moreover, there is a critical value of L over which thermal fluctuations become an important part of the detected signal with a deleterious effect on the sensitivity of the sensor. Even though interferometric sensors are by nature less susceptible to temperature fluctuations due to the compensating effect of the reference arm, there still exists temperature-induced noise because of the dependence of the sensing arm effective refractive index N_s and the cover medium's refractive index n_c on temperature. In order to estimate the magnitude of the thermal fluctuation induced noise, one may assume that the effective refractive index sensitivity to temperature fluctuations is the same as in the

Please cite this article as: Makarona, E., et al., Point-of-Need bioanalytics based on planar optical interferometry, Biotechnol Adv (2016), http://dx.doi.org/10.1016/j.biotechadv.2016.02.005

case of ring resonators (White and Fan, 2008; Misiakos et al., 2014a). Under this assumption, the phase noise may be calculated through:

$$\sigma\varphi_t = 2\pi L\sigma\lambda_t \frac{\partial(N_s/\lambda)}{\partial\lambda} \quad (8)$$

where $\sigma\lambda_t = 10$ fm for the standard deviation value of the ring resonator case (White and Fan, 2008). The thermal fluctuation phase noise is linearly proportional to the size L of the interferometer, setting a practical limit to the design according to the targeted sensitivities. Finally, since the waveguides of the sensors are patterned by photolithography followed by etching processing steps, there always exists a certain line edge roughness (LER). LER is commonly of submicrometer to the several-tens-of nanometer scale, and can have a severe effect on the propagation light through a scattering of the guided beams at the interfaces of the waveguides. Therefore, depending on the order of magnitude of the scattering losses, L has to be kept within values that do not affect in a profound way the propagation of the guided beams as a compromise between sensitivity and transmission losses. Still, L is a parameter along with the other opto-geometrical characteristics of the waveguides that allow for a larger flexibility in the design compared to other types of IOs (such as ring resonators or SPR).

In the following subsections, several MZI and YI sensors will be presented in order to demonstrate their flexibility in terms of material choice, configurations, and design as well as their analytical capabilities and limitations which are directly related to their architecture.

2.2.2. Single-wavelength Mach–Zehnder interferometry implementation

2.2.2.1. Early developments of Si-based SW-MZI sensors. The development of the semiconductor industry has provided scientists with the means to fabricate IO sensors of small size, compatible with mass-production techniques and with the design flexibility necessary to target specific applications. Even from the early '90s motivated by the theoretical predictions that IO sensing, and, in particular, interferometric methods, can provide improved limits of detection compared to other techniques, the first Si-based interferometers made their appearance. Another advantage offered by the Si-based materials is the high index of refraction contrast (~0.5) necessary for effectively guiding light through total internal reflection. The majority of waveguide structures employed by Si-based interferometric sensors have SiO_2 cladding layers ($n \sim 1.46$) and Si_3N_4 or Silicon Oxynitride (SiON) waveguiding layers ($n \sim 2$). Several types of waveguides have been exploited such as slab, strip, rib, anti-resonant reflecting optical waveguides (ARROW) and slot ones (see schematics of Fig. 1c–g), each one offering its own advantages.

One of the earliest works (Heideman et al., 1991), that exhibited the great potential of interferometry as a bioanalytical tool, employed "simple" slab 100 nm-thick Si_3N_4 waveguides with SiO_2 cladding layers. The sensing area was defined by 1 cm-long openings of the upper cladding layer (in this particular example also the reference arm was exposed to the buffer medium) and the light of a He–Ne laser ($\lambda = 632.8$ nm) was in- and out-coupled via gratings crafted onto the chip. This early SW-MZI sensor despite its relatively simpler geometry was able to detect the binding of human Chorionic Gonadotropin (hCG) at a concentration of 25 nM on the anti-hCG antibody-modified sensor, which was equivalent to a refractive index change $\Delta N_{rs} = 1.9 \times 10^{-5}$ RIU, while the phase drift due to thermal and system fluctuations was measured to be $\Delta\varphi/\Delta t = 0.06\ \pi$/h or $\Delta N_{rs}/\Delta t = 2 \times 10^{-7}$ RIU/h. Further refinement of the system with the same waveguide structure and a total chip size of 3×1.5 cm^2 (Heideman et al., 1993) led to a reduced phase drift of $\Delta\varphi/\Delta t = 1 \times 10^{-2}\ \pi$/h directly translated to a minimum detectable effective index change of $\Delta N_{rs} = 6.33 \times 10^{-7}$ RIU and the successful determination of hCG binding to the anti-hCG antibody-modified sensor from a solution of 50 pM within 20 min.

Towards the end of the same decade, several configurations employing rib-waveguide structures explored the bioanalytical capabilities of Mach–Zehnder interferometers for label-free settings. Brosinger et al. (1997) using 350 nm-thick, 2 μm-wide and 55 nm-high ribs SiON waveguides with SiO_2 cladding layers achieved refractometric detection of water–ethanol solutions with a sensitivity $S_c = \Delta\varphi/\Delta n_c = 2.64 \times 10^3\ \pi$RIU^{-1} (assuming a minimum detectable phase change of $\Delta\varphi_{min} = \pi/20$ or else $\Delta n_{c,min} = 1.8 \times 10^{-5}$) and the determination of 2,4-dichlorophenoxyacetic acid (2,4-D) through a competitive immunoassay at concentration as low as 1 μg/ml. Their sensing arm length was $L_{sens} = 12$ mm and their input source a He–Ne laser. At the same time, Schipper et al. (1997a,b) employing Si_3N_4 rib waveguides (4 μm-wide with $t_{rib} = 3$ nm) with SiO_2 cladding layers explored the effect of the core thickness, ranging from 100 nm to 400 nm, on the sensitivity. As expected the thinner waveguides provided the highest sensitivities since the evanescent field can extend into the over-cladding area and thus "probe" more effectively the cover medium and/or the forming adlayer. With a sensing area length of $L_{sens} = 5$ mm, and the standard He–Ne laser as the input source, a fitted sensitivity of $S_c = \Delta\varphi/\Delta n_c = 2.8 \times 10^3\ \pi$RIU^{-1} was obtained through refractometric sensing of aqueous glucose solutions. Immunodetection of hCG by sensors modified with an anti-hCG antibody gave a detectable signal at a concentration of 30 nM and saturation after the sequential addition of hCG solutions with concentrations of 60 and 80 nM. Nevertheless, the exact LOD was not determined.

2.2.2.2. SW-MZI limitations. Despite the very promising results, the intrinsic limitations of the MZI method along with external limiting factors soon became apparent (these limitations equally apply to YIs). These limitations are:

(*I.1*) *Phase* (*fringe order*) *ambiguity*: for any power ratio I_{out}/I_{in} any solution $\Delta\varphi_k = \Delta\varphi + 2k\pi$, with k being an integer, is an equally probable solution.

(*I.2*) *Directional ambiguity*: it is not possible to deduce the direction of phase change from the MZI transfer function.

(*I.3*) *Signal fading*: because of the sinusoidal nature of the MZI transfer function (see Eq. (5)) operation near the extrema (minima or maxima) results into decreased sensitivity since the derivative is almost zero. Care must be taken to avoid operation near the extrema and to ensure that the sensor operates near the quadrature points, a fact that renders the design application specific and counteracts the otherwise design flexibility of the interferometric sensors.

In addition to the inherent limitations imposed by the very nature of MZI, there are several external factors that may limit the performance of the sensor and reduce its sensitivity and resolution:

(*E.1*) *Fabrication imperfections*: these may include non-uniformity of the waveguide thickness, non-accurate control of the rib height (in the case of rib waveguides which require nm-precision during the etching step), line edge roughness from the lithographic steps, and, in general, are related to the tolerances of each fabrication step. These imperfections collectively result into a reduced fringe visibility directly translated to reduced resolution.

(*E.2*) *Instabilities of the input source*: laser shot noise or spectral bandwidth contribute to the uncertainty of the phase signal with a direct impact on resolution and LOD.

(*E.3*) *Detector noise*: MZI is inherently an intensity measurement-based method. The noise level of the detector (usually a photodiode) sets a limit to the minimum detectable phase change.

(*E.4*) *Coupling losses*: the interferometric sensors have to be coupled both to the input source and to the detector usually through optical fibers and with the aid of several optical components such as objective lenses, grating couplers, and polarizers. Hence, in order to minimize the losses, special care has to be devoted to the development of the optical system in order to maximize the coupling efficiencies.

Please cite this article as: Makarona, E., et al., Point-of-Need bioanalytics based on planar optical interferometry, Biotechnol Adv (2016), http://dx.doi.org/10.1016/j.biotechadv.2016.02.005

(*E.5*) *Thermal fluctuations*: in general temperature fluctuations are counter-balanced in an integrated interferometric sensor, because it is actually a self-referenced device while the two branches are closely spaced (usually, they are placed within 20–100 μm) and the temperature gradients are rather small. In addition, Si wafers have a high thermal conductivity adding to the thermal stability of the sensor. Nonetheless, when the detection limits are pushed to the lowest possible values, especially in the case of sensing of protein monolayer fraction, even the more minute temperature fluctuations can affect the LOD of the sensors. In a sense, the inherent high sensitivity of the interferometric sensors imposes a limit on itself, since it is capable of detecting very small temperature fluctuations that can be comparable to the actual sensing signal.

For all the above reasons, several schemes have been devised in order to counteract for one or more of these limiting factors. Heideman and his co-workers (Heideman and Lambeck, 1999) suggested the use of an electro-optical modulator for active-phase modulation in order to circumvent the phase ambiguity and signal fading issues while enhancing immunity to external noise factors. The proposed serrodyne type modulation method led (using a He–Ne laser source) to a phase resolution of $\Delta\varphi_{min} = 2 \times 10^{-4}$ π equivalent to an effective refractive index resolution of 5×10^{-8} RIU and a long-term stability of 10^{-7} RIU. Gauglitz' group (Drapp et al., 1997) devised the use of a 3×3 coupler at the output of the MZI. Instead of recombining the two light beams of the interferometer in a simple Y-junction, mode coupling was used to exchange power from the two arms between the three outputs phase shifted by 2π/3 from each other, and thus ensure that at least one of the 3 outputs would operate near a quadrature point. An additional advantage of this scheme was the fact that referencing the output signal allowed the elimination of signal fluctuations due to coupling and light-source instabilities and resulted in an increase in the signal-to-noise ratio by a factor of up to 10 compared to the conventional MZI configuration. Though the particular MZI was not realized on a Si wafer, but on a BGG36 glass substrate with a refractive index of 1.6009 at 588 nm, microelectronic processing techniques were employed (such as lithography, CVD deposition of SiO_2 and etching steps) for its fabrication. A detection limit for a change in cover refractive index of $\Delta n_c = 1.5 \times 10^{-6}$ RIU was determined from the three-fold rms noise. This alternative multiple-output MZI was used for simazine detection, and significant inhibition of antibody binding was detected even at analyte concentrations in the sub-ppb range. The LOD was evaluated to be 0.1 ng/ml.

2.2.2.3. Enhancing the sensitivity of Si-based SW-MZI sensors. The beginning of the new millennium found the research society actively pursuing strategies to improve the sensitivity of interferometric sensing. The Lechuga group followed in parallel two routes. On the one hand, MZIs with 4 μm-wide Si_3N_4 cores, a 4 nm-high rib, and SiO_2 cladding layers were fabricated with silicon technology (Prieto et al., 2003). The MZIs with 15 mm-long sensing arms were tested using the TM polarization of a He–Ne laser against aqueous solutions of HCl (Blanco et al., 2006). From these refractometric measurements a LOD of $\Delta n_{c,min} = 3.8 \times 10^{-6}$ RIU or equivalently $\Delta N_{rs,min} = 2 \times 10^{-7}$ RIU was achieved. By extrapolating the sensitivity curve and given that the lowest detectable phase change of the system was $\Delta\varphi_{min} = 0.1 \times 2\pi$, a phase sensitivity of $S_c = \Delta\varphi/\Delta n_c = 3720 RIU^{-1} = 1.184 \times 10^3 \times \pi\ RIU^{-1}$ was made possible. On the other hand, ARROW structures, Fig. 1f, based on silicon technology were extensively simulated and analyzed (Prieto et al., 2000) with a prediction for adlayer sensitivities of $S_{ad}^{TE} = {}^{\partial N_{rs}^{TE}}/_{\partial t_{ad}} = 0.06 \times 10^{-4} RIU/nm$ and $S_{ad}^{TM} = {}^{\partial N_{rs}^{TM}}/_{\partial t_{ad}} = 3.4 \times 10^{-4} RIU/nm$, for TE and TM polarized light respectively. ARROW-based MZIs were tested (Prieto et al., 2003) by varying not only the sensing area length (L_{sens} = 6, 10, 15, and 20 mm) but also the nitride core thickness (t_{core} = 46, 60, and 120 nm), since according to the nature of evanescent sensing, thinning of the core increases the penetration depth of the evanescent field, and hence the sensitivity. MZIs with ARROW structures and $L_{sens} = 10$ mm achieved a LOD of $\Delta n_{c,min} = 10^{-4}$ RIU or equivalently $\Delta N_{rs,min} = 2 \times 10^{-6}$ RIU when used as refractometers with water/glucose solutions. In addition, MZIs with ARROW structures and $L_{sens} = 15$ mm were exploited for the detection of human serum albumin (HSA) through the immobilization of an anti-HSA antibody and found able to detect down to 7.7 μM of antigen which is equivalent of an adlayer build-up of $t_{ad} = 1.8$ nm.

Exploring the potential of ARROW structures, another approach using porous Si in place of silicon nitride or oxynitrides was also realized (Hiraoui et al., 2012) in order to employ telecom wavelengths. Buried 4 μm-wide ARROW waveguides developed on heavily doped p-type Si were fabricated and various porosities and core thickness were investigated. When ethanol was left to evaporate on the 5 mm-sensing area of the MZI (corresponding to a refractive index change of $\Delta n_c = (2.48 \pm 0.31) \times 10^{-3}$ calculated by Eq. (6) with $\lambda = 1.55$ μm) 16 fringes were detected.

Another way to optimize an MZI performance is to minimize optical transmission losses through fine-tuning of the divisors that split and recombine the two traveling beams. S-bends versus angular Y-junctions were extensively simulated (Sarkar et al., 2013) for nitride-based rib waveguides with SiO_2 cladding layers. Several opening angles for the angle Y-junctions and several radii of curvature for the S-bend junctions were examined while keeping the total size of the MZI sensor and the distance between the two arms constant. This meant that according to the shape and size of the Y-divisor angles the sensing area size would vary accordingly. The simulation results indicated that in general angular bends with $\theta < 2.5^o$ and S-bends with $R_{bend} > 15$ mm experience lower losses. Experimentally, MZIs with S-bends of a 56-mm radius of curvature were employed with 250 nm-core thickness, 4 μm-wide rib waveguides of 4 nm-ribs and a sensing area of 15 mm (Sarkar et al., 2014). The final chip footprint was 1.5×30 mm^2 and was applied to the detection of *Listeria monocytogenes* by performing power measurements at the input and output end of the MZI chips. The minimum detectable concentration was 2.8×10^5 CFU/ml, which is well below the infective dosage of *L. monocytogenes* for humans and better than the LOD achieved by most of the alternative detection methods. An upper limit of 2.8×10^{10} CFU/ml was found, at which point the normalized power intensity value was invariant to the change in *L. monocytogenes* concentration, providing however for a dynamic range of 5 orders of magnitude.

In the continuous effort to improve the LODs of SW-MZIs, slot waveguides were exploited, Fig. 1g. Liu et al. (2014) fabricated Si_3N_4-based waveguides with SiO_2 cladding layers. The waveguide of the sensing area was substituted by a slot waveguide while the reference arm maintained the more standard rib-waveguide configuration. Thanks to the slot waveguide's property to provide high optical intensity in a sub-wavelength-size low refractive index region (slot region), which enhances light-analyte interaction, higher sensitivities were obtained as compared to conventional waveguides. Additionally, the designed MZIs had a spiral configuration of the arms in order to increase the interaction length to 7 mm, while keeping the chip final footprint as small as possible. A tunable laser emitting at = 1.56 μm was used as the input source. Testing with aqueous NaCl solutions established a phase sensitivity of $\Delta\varphi/\Delta n_c = 1.864 \times 10^3 \pi\ RIU^{-1}$. With a minimum detectable phase change $\Delta\varphi_{min} = 0.01$ π, a LOD of 5.4×10^{-6} RIU in terms of bulk refractive index changes was calculated. Affinity sensing with the biotin-streptavidin binding assay reached a LOD of 18.9 fM (or 1 pg/ml) of streptavidin. In effort to translate the analytical detection capability of the slot-MZI to surface density, the authors also performed the following calculations: The real-time optical response due to adsorption of 5.0 μg/ml (95 nM) streptavidin to the biotinylated sensor surface resulted in a phase change of 10.6 π for an interaction length of 7 mm or else a phase change to the interaction length of 14.7 π/cm. As the surface density of the streptavidin was known to be 2.33 ng/

Please cite this article as: Makarona, E., et al., Point-of-Need bioanalytics based on planar optical interferometry, Biotechnol Adv (2016), http://dx.doi.org/10.1016/j.biotechadv.2016.02.005

mm^2 the mass sensitivity was calculated to be ~4.55 π/(ng mm^{-2}). Finally, in order to demonstrate the great potential of the slot-MZI for a large variety of biosensing applications, the same device was employed for the specific detection and quantification of the methylation of DAPK gene, which is associated with the recurrence and metastasis of several human cancers. The phase change was measured after hybridization with matched and mismatched target sequences to DNA probes immobilized onto the MZI slot waveguide. It was found, that the sensor was able to distinguish among three types of methylation density (100%, 50%, and 0%) even when the concentration was as low as 1 fmol/μl (1 nM), a performance 3 orders of magnitude better than microring resonators. The same group, very recently (Liu et al., 2015) combined the proposed slot-MZI with isothermal solid-phase amplification (IDA). The system was used to detect an L858R mutation in Epidermal Growth Factor Receptor (EGFR), a non-small-cell lung cancer (NSCLC) biomarker. The system achieved an impressive detection of L858R mutation in a 99:1 mixture of wild-type and mutant cells. Moreover, in a pilot clinical study, the system was compared to conventional methods (PCR and direct sequencing) using tissue biopsy samples from NSCLC patients. The slot-MZI-IDA system was proven not only capable of fast and accurate detection of the L858R mutation of EGFR gene in clinical samples but achieved a LOD of 0.125 pg/μl, which was 3 orders of magnitude lower than that of gel electrophoresis analysis of PCR products.

2.2.2.4. Polymer-based SW-MZI sensors. In the previous section, the short overview of Si-based SW-MZIs was used to demonstrate their large potential for highly-sensitive biosensing applications. The realization of SW-MZI with standard silicon microelectronics/micromachining technologies offers the clear advantage of mass production at high volumes with well-established processing techniques. However, silicon devices cannot be considered as fully-disposable parts, and if they are to be used as core elements of a PoN system further studies are required in order to devise strategies and biofunctionalization protocols that may render them re-usable (see also discussion in Sections 3 and 4). For that reason, it is of particular interest to fabricate fully-disposable optical sensing chips that should also be able to deliver analytical performance equivalent to the one from the silicon based interferometric chips. A straight forward approach in that direction is the design and realization of all polymer optical sensing chips, an approach that has the obvious advantage of easy integration of the fluidic cells that are also used in the silicon chips.

In this approach, the planar waveguides are not fabricated from silicon or silicon nitride but from polymers with appropriate refractive index contrast. The refractive index contrast that can be achieved with polymers is rather low (few hundredths or very few tenths of RIU) unlike the silicon based waveguides, where a refractive index contrast of ~0.5 can easily be achieved by employing SiO_2 and Si_3N_4 layers. Because of this low refractive index contrast between the core and the cladding layers, the single mode polymeric planar waveguides have a width of several micrometers. In addition, polymers are quite sensitive at processing and the realization and patterning of polymeric layers with high quality is a difficult task that requires significant engineering work.

The selection of the polymeric materials is based on the wavelength of operation with most polymeric interferometric sensor to have been realized for operation in the standard wavelengths of 633 nm (He–Ne laser), 1310 nm or 1550 nm (telecom wavelengths). The material most commonly used for the realization of polymeric interferometric waveguides is the well-known SU-8 resist, the refractive index of which can be tuned into some extent through UV exposure. However, due to the very low index difference of only few thousandths and the large waveguide thickness of few micrometers, the fabricated sensor can have only a very little surface sensitivity. Another typical polymeric material that has been used as core layer is polyimide (n ~ 1.65).

The all-plastic interferometric structures (Bruck et al., 2011; Shew et al., 2008; Dér et al., 2010; Melnik et al., 2011; Yu et al., 2014) are fabricated either on rigid substrates, e.g., glass or silicon or on plastic substrates. In the latter case, which is the final goal for mass production of low-cost sensing chips, standard industrial polymer processing methods such as injection molding and hot embossing could be used. However, at research level, the majority of the plastics interferometric structures are realized on standard Si substrates with thick (several microns) silicon oxide layers. Theoretical studies (e.g., Bruck et al., 2011) have shown that exactly due to the low refractive index contrast the expected sensitivity of a polymeric interferometer is approximately one order of magnitude lower from that of sensors based on silicon (silicon nitride and silicon dioxide) technology. However, the final analytical performance depends strongly on the biofunctionalization properties of the layer used as the core.

The fabrication of the polymeric interferometric structure follows the standard microelectronic processing techniques (Shew et al., 2008) and in particular: the bottom cladding (thickness of several microns) is formulated through the spin coating of the SU-8 photoresist followed by the standard lithographic procedure of Post Apply Bake and Flood Exposure. Then a new layer of SU-8 resist with the same thickness as the bottom cladding layer was applied and patterned through an appropriate mask in order to realize the interferometric structure, i.e., the Y-splitters and the reference and sensing arms. Then both resist layers (the bottom cladding and the patterned one) are cured at a high temperature in order to reach a refractive index value of approximately 1.570. The next processing step is the spin coating of an additional SU-8 layer to serve as the core of the waveguide. This layer is processed with the standard lithographic procedure (Post Apply Bake, Flood Exposure, Post Exposure Bake) that allows for a cross-linking density that will ensure tolerance of the next processing steps involving activation and immobilization of biomolecules. This way a refractive index contrast of 0.004 is achieved. The optical evaluation of the chip showed optical losses less than 6 dB. Measurements with model assays (rabbit IgG/anti-IgG antibody) showed that is possible to reach sensitivities of 1 ng/ml (ca. 6.7 pM), which is comparable with the corresponding values for standard silicon SW-MZIs. Thus, polymeric interferometric sensors could be a viable solution for the fabrication of disposable SW-MZI sensors.

2.2.3. Single-wavelength Young interferometry implementation

Despite the great interest of the research community over the last two decades on interferometric techniques for PoN applications, Young interferometry – curiously enough – has not attracted an equal share of interest compared to Mach–Zehnder interferometers. Despite the fact that as a technique is relatively simpler to implement, and requires only an imaging device, such as a CCD array, to detect the interferogram, the number of publications devoted to Young interferometers are considerably less numerous. Also, the fact that with YI more information can be obtained compared to conventional MZIs, because an entire intensity profile is detected instead of a single intensity value, adds to this conundrum. This puzzling aspect will be further discussed in Section 4, while this sub-section will mainly focus on the performance of YIs developed so far.

One of the first attempts to implement YIs as optical sensors was presented by Brandenburg and Henninger (1994), who fabricated an integrated optical device by thermal K^+–Na^+ exchange in a borosilicate glass. Instead of using coherent light, partially coherent light from a laser diode ($\lambda = 783$ nm) operating below the laser threshold was employed, in order to circumvent the phase ambiguity problem resulting in visibility modulation of the interference fringes caused by the low coherence length of the emitted light. The problem of ambiguity is solved by analyzing the function's envelope through FFT. Further elaboration of the approach (Brandenburg, 1997) resulted in an impressive LOD for bulk refractive index measurements with aqueous saccharose solutions of $\Delta N_{eff,min} = 5 \times 19^{-9}$ RIU corresponding to the noise level of the baseline. Even if one considers that the actual LOD would be 3 times the noise level, still this would correspond to a LOD of $\Delta N_{eff,min} = 1.5 \times 19^{-8}$ RIU, one of the best-recorded values so far.

Please cite this article as: Makarona, E., et al., Point-of-Need bioanalytics based on planar optical interferometry, Biotechnol Adv (2016), http://dx.doi.org/10.1016/j.biotechadv.2016.02.005

Feasibility studies for real-life clinical settings were also performed later, with YIs being employed for detection of antibodies in blood plasma (Brynda et al., 2002) with Si_3N_4/SiO_2-based YIs on Si chips (Brandenburg et al., 2000) and tuberculosis-specific antibodies in human blood serum (Nagel et al., 2008) with commercial Ta_2O_5-YIs on glass (Unaxis Balzers, Liechtenstein) providing results at clinically relevant values.

During the same period of time, a Ta_2O_5-waveguide on glass YI chip was used by the same group (Hoffmann et al., 2007). The sensor chip consisted of a 0.7 mm-thick glass substrate coated with a waveguide layer of Ta_2O_5 with a thickness of 154 nm and a refractive index of 2.1. Light from a red super-luminescence diode emitting at 675 nm was split into two beams and coupled into the waveguide by a grating. The two outcoming beams were coupled out by a second grating, passed a double slit, interfered in the far field, and detected by a CCD camera. A LOD of $\Delta N_{eff,min} = 9 \times 10^{-8}$ RIU was obtained equal to the threefold of the noise level. The standard curve obtained for detecting a protein engineered with a Novartis Proprietary Tag (NPT) to immobilized onto sensor anti-NPT antibody showed a limit of quantitation (tenfold noise level) of 8.3 ng/ml (400 pM). In parallel, Schmitt et al. (2007) employing the same Ta_2O_5-based YI and optical setup configuration, yielded a LOD of effective index of refraction $\Delta N_{eff,min} = 9 \times 10^{-9}$ RIU (corresponding to a bulk refractive index change of $\Delta n_c = 4 \times 10^{-8}$ RIU) as determined using aqueous glycerine solutions. This impressive LOD is – to the authors' best of knowledge – the lowest reported value not only in Young interferometry but in general in interferometric sensors, and has thus set the limit that the next generation of sensors needs to surpass. In the same publication (Schmitt et al., 2007), the YI was applied to monitor the binding of protein G with immunoglobulins G (IgG). A concentration of 270 pM IgG was unambiguously detected while taking into consideration the refractometric LOD of 9×10^{-9} RIU, the authors extrapolated a projected LOD for IgG as low as 390 fM.

In addition, a different approach to the notion of future multi-analyte, multiplexed operation of YIs, was developed by Ymeti et al. (2003), who fabricated a four-channel YI where monochromatic laser light is coupled into an input channel waveguide and equally split into N output parallel channels. As the output divergent beams overlap with one another, the final interference pattern recorded by a CCD camera is a superposition of individual interference patterns, each of them representing the overlap of the divergent beams of a specific channel pair. Each pair of beams will produce an individual interference pattern with a spatial frequency:

$$k_{ij} = \frac{b_{ij}}{\lambda D} \tag{9}$$

with b_{ij} the distance between the ith and jth channel for the chip. Each k_{ij} will appear as a distinct peak in the FFT of the interference pattern providing an equally distinct value for the phase difference among the various pairs of channels given by:

$$\Delta\varphi_{ij} = \frac{2\pi L}{\lambda}\frac{\partial N_{eff}}{\partial n_c}\Delta n_{ij} \tag{10}$$

where Δn_{ij} is the difference of the cover refractive index of the ith and jth channel. Any change in Δn_{ij} causes a spatial shift Δyij in the individual interference pattern for this channel pair. From the phase part of the Fourier transformation, the phase value $\Delta\varphi_{ij}$ for each specific spatial frequency can be extracted, measuring in such a way the phase difference between the channels of each channel pair of the multichannel device. Applications of this approach with chips fabricated with standard Si processing (Si_3N_4 waveguides with SiO_2 cladding layers on Si wafers) yielded a minimum detectable effective index of refraction with aqueous glucose solutions of $\Delta N_{eff,min} = 6 \times 10^{-8}$ RIU being equivalent to a protein mass coverage resolution of 20 fg/mm^2 as estimated by the authors though measurements of Human Serum Albumin (HSA) binding on an anti-HSA antibody modified sensor (Ymeti et al., 2005). Furthermore, the performance of the sensor was evaluated by monitoring the coupling of virus solutions at clinically relevant concentrations by sensors modified with an anti-virus specific antibody (Ymeti et al., 2007). It was shown that it is possible to detect HSV-1 (herpes simplex virus type 1) at very low concentrations (850 particles/ml) as well as to detect HSV-1 suspended in serum. Extrapolation of the results by the authors predicts that it could be possible for the sensor to detect a single virus particle binding; rendering the device suitable for viral diagnostics.

Undoubtedly, YIs have exhibited the best performance so far yielding in general one to two orders of magnitude higher sensitivities than their MZI counterparts and have achieved that with even simpler configurations. It remains to be seen how far more their analytical capabilities can extend and how they can be integrated into marketable systems for PoN applications especially in the field of medical diagnostics.

2.3. Multi-wavelength and broad-band interferometry

In order to develop practical and realistic PoN systems, the detection has to be performed directly on clinically relevant samples, in other words, bodily fluids such as blood, blood plasma or serum, and saliva, which are complex media containing a multitude of biomolecules apart from the targeted analyte, usually found in small amounts (especially in the case that early diagnosis is aimed for). As a result, the high sensitivities that can be achieved with interferometric sensors put a self-limiting factor on the performance, since along with the actual signal, non-specific binding and RI changes of the matrix are recorded simultaneously. In order to address the disadvantages of single wavelength interferometric biosensors that were analyzed in the previous chapter, transducers that are based on spectral interferometry were introduced in 00's. In particular, transduction principles based on broad-band Mach–Zehnder (Luo et al., 2003; Li et al., 2010; Kitsara et al., 2010) and multiple wavelengths Young interferometry (Mulder et al., 2012; Stamm et al., 1998) were designed, implemented and evaluated in real settings.

2.3.1. Broad-band Mach–Zehnder interferometry (BB-MZI)

2.3.1.1. Theory of broad-band Mach–Zehnder interferometry. In broad-band MZI approaches a broad-band light source emits light that is coupled to the planar interferometric transducer and the output spectrum is monitored through an external spectrometer. Luo et al. (2003), have designed and fabricated a BB-MZI chip in which the refractive index contrast between the core and the cladding layers, made from P-doped SiO_2 and SiO_2 respectively, is only ~0.008 while in the standard Si_3N_4/SiO_2 SW-MZI this difference is ~0.5. For the operation of that device, the output of a white light source was coupled to the planar waveguide and the transmitted light was monitored with an external optical spectrum analyzer in the 1200–1700 nm spectral regime. The change in the refractive index of the cover medium of the sensing arm showed clear red shifts in the recorded spectrum and the measured sensitivity was ~4.0×10^{-3}, quite low compared to the sensitivity values recorded by SW-MZI devices. However, this first demonstration of BB-MZIs with ethanol solutions, even though of low sensitivity, solves the SW-MZIs namely ambiguity and signal fading, e.g., by monitoring the interference intensity in each of the wavelengths of the spectrometer.

Few years later Li et al. (2010) introduced the spectrum differential integration MZI where again light in NIR is coupled to a Mach–Zehnder structure and the transmitted interference spectrum is recorded by an optical spectrum analyzer. In this approach, the recorded sensitivity

Please cite this article as: Makarona, E., et al., Point-of-Need bioanalytics based on planar optical interferometry, Biotechnol Adv (2016), http://dx.doi.org/10.1016/j.biotechadv.2016.02.005

was few tens of nanometer per RIU, quite low for biosensing applications.

In parallel Misiakos and co-workers (Kitsara et al., 2010) have proposed the concept of Frequency-Resolved Mach–Zehnder interferometry in the VIS–NIR spectral range and for wider spectral windows. In their theoretical study that was applied to MZI structures with high refractive index contrast between the core and cladding layers, Si_3N_4 and SiO_2, respectively, they have proved that through appropriate waveguide engineering it is possible to reach LOD values down to effective adlayer thickness of 2.5 pm even with sensing area lengths as short as 600 μm.

In all above briefly described approaches the phase ambiguity and signal fading disadvantages of standard SW-MZI transducers are effectively addressed at the expense of the use of broad-band light sources and optical spectrum analyzers or spectrometers. However, to make optical microsystems more robust and cost efficient, monolithic integration of the light sources along with the waveguiding elements is required to avoid the shortfalls associated with hybrid integration approaches. In the later, external light sources have to be coupled to the extremely thin and narrow waveguides through bulk optics, such as lenses, prism couplers, and collimators (Kozma et al., 2014), raising accuracy, reliability and cost issues, especially when portable systems are considered.

For truly monolithic silicon interferometry, the light source has to be integrated on a chip (Misiakos et al., 2004). Although silicon is an indirect band gap material, light emission is possible in properly nanoengineered silicon diodes that incorporate either silicon nanocrystals embedded in a silicon dioxide insulator (Anopchenko et al., 2013), or silicon quantum wires (Nassiopoulos et al., 1995a, 1995b). Another electroluminescent device is the silicon avalanche p/n diode which emits light when biased beyond its breakdown voltage (Chynoweth and Mckay, 1956). All of the above diodes emit a broad spectrum that includes the visible and the near-infrared spectral region. Provided that standard interferometers, like ring resonators or Mach-Zehnder devices, are based on monochromatic light sources, any monolithic silicon optocoupler devices must deal with the broadband nature of the silicon-based light sources. This is done by choosing the Mach–Zehnder configuration with properly engineered sensing and reference arms. There are two modes of operation for such a device: In the first one (termed hereafter for simplicity "fully-integrated"), the sensing and reference arm effective indices are chosen so that the phase difference of the light travelling through them is more or less wavelength independent in the emission spectral range of the light emitting diodes (Misiakos et al., 2014a). This is realized by choosing the right core thicknesses of the two arms. Such a device can accommodate broadband light through the well-known sinusoidal expression for the detected intensity as a function of the sensing-reference arm effective index difference, as in the case of Mach–Zehnder devices that employ monochromatic light (Eqs. (5) and (6)):

$$T = \frac{I_{out}}{I_{in}} = \frac{1}{2}\left[1 + \cos\left(2\pi\frac{\Delta N_{rs}}{\lambda}L\right)\right] \tag{11}$$

In Eq. (11), T is the transfer function as the ratio of the output (I_{out}) over the input (I_{in}) power and ΔN_{rs} is the difference between the effective indices of the reference, N_r, and the sensing, N_s, arms. The term L is the exposed arm length. With the right selection of the two arms thickness the ratio $\Delta N_{rs}/\lambda$ becomes more or less wavelength independent rendering T constant throughout the waveguided spectrum. An integrated photodetector can provide direct results on the photocurrent intensity as a sinusoidal function of the sensing-reference arm effective index difference (Misiakos et al., 2014a).

In the second mode of operation (termed hereafter for simplicity "semi-integrated"), the sensing arm is thinned with respect to the reference one so that the ratio $\Delta N_{rs}(\lambda)/\lambda$ and the transfer function $T(\lambda)$ are functions of the wavelength (Misiakos et al., 2014b). Now the observable is the spectral shifts, $\delta\lambda$, caused by sensing arm effective index change δN_s:

$$\delta\lambda = \frac{\delta N_s(\lambda)}{\lambda\left[-\frac{\partial(N_s/\lambda)}{\partial\lambda} + \frac{\partial(N_r/\lambda)}{\partial\lambda}\right]} = \frac{\delta N_s(\lambda)}{\lambda\left[\frac{\partial(\Delta N_{rs}/\lambda)}{\partial\lambda}\right]} \tag{12}$$

In the right hand side in Eq. (12) the denominator term is two orders of magnitude smaller than the denominator the similar equation for the spectral shift in the case of a standard ring resonator:

$$\delta\lambda = -\frac{\delta N_s(\lambda_r)}{\lambda_r\frac{\partial(N_s/\lambda)}{\partial\lambda}} \tag{13}$$

Consequently, the spectral shifts obtain from a Mach–Zehnder broad-band interferometer are two orders of magnitude larger compared to similar shifts in ring resonators (Misiakos et al., 2014b). Such large spectral shifts can be readily recorded by modern portable spectrometers opening the way of using white light modulation through Mach–Zehnder interferometry as a transduction principle in point of care bioanalytical microsystems.

Through proper photonic engineering of the two arms, namely by thinning the sensing arm with respect to the reference arm, the ratio $\Delta N_{rs}(\lambda)/\lambda$ can be made nearly linear with respect to λ in the spectral range of interest (Misiakos et al., 2014b):

$$\Delta N_{rs}(\lambda)/\lambda = a\lambda + b \tag{14}$$

so that Eq. (11) can be rewritten

$$T(\lambda) = 0.5\cdot[1 + \cos(2\pi(a\lambda + b)L)] \tag{15}$$

The terms a and b are the slope and the zero λ intercept of the $\Delta N_{rs}(\lambda)/\lambda$ function. Considering the Mach–Zehnder interferometer as a resonator, the Free Spectral Range (FSR), FWHM and Q factor become $1/(La)$, $1/(2La)$, $2La\lambda$, respectively. Here, and as opposed to a ring resonator, one does not track a sharp resonance at a specific wavelength but rather a broadband spectrum is recorded through spectrometers the spectral resolution of which needs only be much smaller than the free spectral range. The spectral shifts are derived from the entire recorded spectrum so that effective resolutions in the pm range are possible even though portable commercial spectrometers with nm range resolution are employed. The sinusoidal nature of the transfer function in Eq. (15) facilitates the spectral shift study. The use of Discrete Fourier Transform (DFT) in such an output spectrum leads to a dominant peak in the wavenumber domain and the phase is identified with the argument of the complex DFT value at the main peak while white noise is filtered by ignoring non-resonant frequencies in the spectrum. The peak will appear at $2\pi aL$ and the phase at the peak is $2\pi bL$. The oscillation frequency determining slope factor a is polarization dependent and two distinct peaks will appear at different positions in the DFT domain when both polarizations are multiplexed at the input of the interferometer. Peak splitting may also allow for simultaneous demultiplexing of either polarization enabling in-depth analysis of adlayer formation and distinction between bulk refractive index changes and adlayer-induced effective refractive index changes in a manner analogous to the dual-polarization schemes introduced by Lukosz (Tiefenthaler and Lukosz, 1989).

2.3.1.2. Implementation of broad-band Mach–Zehnder interferometry. The broadband device described above is monolithically implemented on silicon as shown in Fig. 2a. Light emitting diodes (LEDs) and silicon nitride planar waveguides are monolithically integrated and optically coupled on a silicon wafer. The LEDs are silicon avalanche diodes that emit white light in reverse bias and beyond breakdown. The

Please cite this article as: Makarona, E., et al., Point-of-Need bioanalytics based on planar optical interferometry, Biotechnol Adv (2016), http://dx.doi.org/10.1016/j.biotechadv.2016.02.005

integration of the active and passive optical components is achieved by employing mainstream planar technology and self-alignment techniques that allow efficient coupling between the LED and the waveguide (Misiakos et al., 2014b). The LED P^{++} emitter is implanted through the silicon nitride layer, the boron atoms compensate the pre-existing base N^+ implant so that the metallurgical junction of the LED is precisely placed under the up-going segment of the waveguide. The SiO_2 spacer next to the LED provides for the smooth waveguide bending and minimizes bending losses. The light is first coupled to a multimode silicon nitride waveguide, then goes through a mode filter followed by the Mach-Zehnder interferometer before it delivers the modulated signal to the spectrometer through an external fiber; semi-integrated configuration. In the fully-integrated version, the waveguides all converge through a second spacer to photodiode monolithically-integrated and self-aligned to the waveguides in a manner similar to the LEDs. In both configurations, a fluidic compartment on top of the exposed sensing waveguide allows for the supply of the sample and the reagents.

For the fully-integrated version, the photocurrent from the monolithically integrated photodiode was measured, while the phase change was calculated through

$$\Delta\varphi = arc\ \cos\left(\frac{I_{ph}-I_{spp}}{I_{dpp}}\right) \tag{16}$$

where I_{spp}, I_{dpp} are the semi-sum, $(I_{max} + I_{min})/2$, and semi-difference, $(I_{max} - I_{min})/2$, of the highest (I_{max}) and the lowest values (I_{min}) of the recorded photocurrent (I_{ph}). The introduction of the semi-sum and semi-difference photocurrent values are necessary to isolate the dc component of the photocurrent transient (Misiakos et al., 2014a). Taking into account that the rms of the photocurrent noise was $I_{noise,\ rms} = 19fA$, a LOD of $\Delta N_{min} = 5 \times 10^{-6}$ was calculated. To demonstrate its capabilities for multi-analyte PoN applications, a chip containing an array 10 BB-MZIs all with their broadband input source all converging to a common photodetector was used for the simultaneous detection of anti-mouse IgG-mouse IgG and biotin-streptavidin binding. Four out of 10 BB-MZIs were spotted with mouse IgG, three with biotinylated BSA, and the remaining three with blank BSA to serve as controls. Successful simultaneous detection in a multiplexed format of 10 nM of anti-mouse IgG and 1 nM of streptavidin was realized.

In the semi-integrated BB-MZI case, in terms of signal to noise ratio, the fundamental noise source is the shot noise in each of the digital spectrometers channels. As mentioned above, the signal is the phase shift at the Fourier transform peak in the wavenumber domain and appears at $2\pi aL$. If P_c is the total number of photons entering the interferometer in each recording, a shot noise analysis provides for the phase noise (Misiakos et al., 2014b):

$$\sigma\varphi = \frac{2}{\sqrt{P_c}} \tag{17}$$

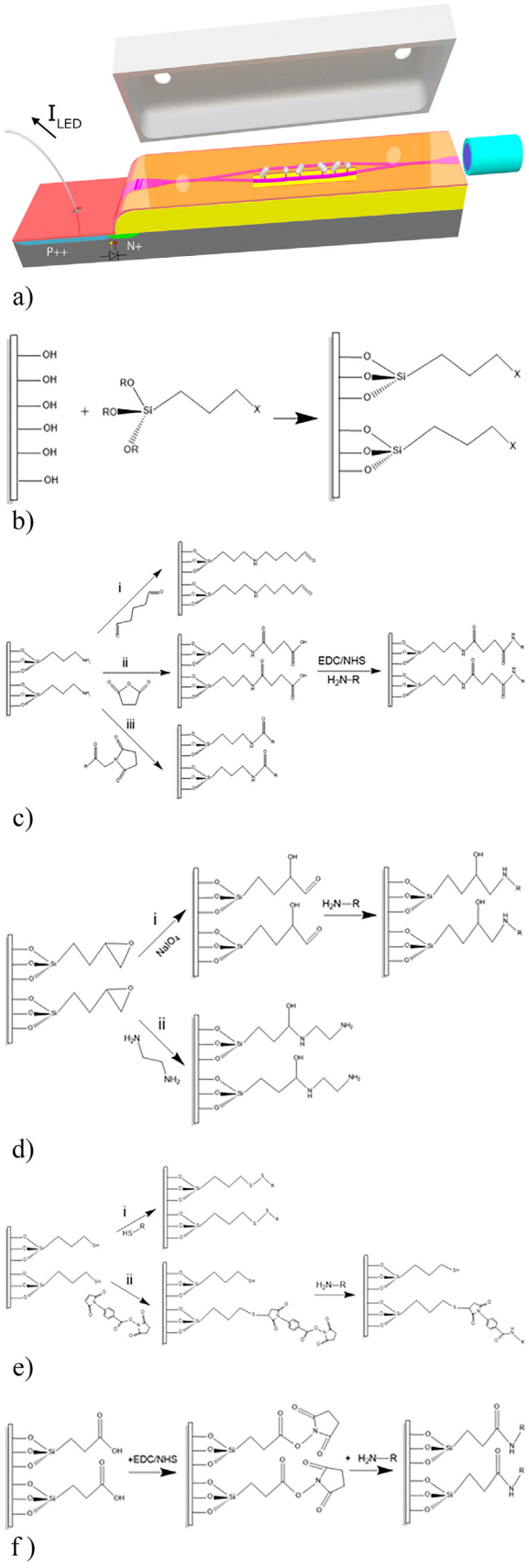

Fig. 2. (a) Silicon chip with a monolithically integrated broad-band Mach–Zehnder interferometer. The schematic shows the monolithic integration of the avalanche-type LED, the Mach–Zehnder interferometer. The N^{++} emitter (purple) forms the metallurgical junction with the P^+ base (yellow) just under the up-going segment of the silicon nitride waveguide (pink). The SiO_2 quadrant spacer with the broken line is employed to reduced waveguide bending losses. The single mode rib waveguides have a width of 1.25 μm and an etch depth of 4 nm. The sensing arm thickness is 150 nm. The chip emitting edge is coupled to an external spectrometer, through an optical fiber. The probe molecules are immobilized on the exposed sensing arm. The cover on top indicates the fluidic compartment. (b) Reaction scheme of silicon-based surface functionalization with organosilanes. (c) Attachment of biomolecules on surfaces modified with amine-terminated silane through activation with (i) glutaraldehyde, (ii) succinic anhydride, or (iii) reaction with N-hydroxysuccinimido-esters. (d) Attachment of biomolecules on surfaces modified with epoxy-terminated silane after (i) oxidation to carbonyl groups, or (ii) reaction with ethylendiamine to convert epoxy- to amine-groups. (e) Attachment of biomolecules on surfaces modified with thiol-terminated silane through (i) thiol–thiol interaction, or (ii) m-maleimidobenzoyl-N-hydroxysuccinimide. (f) Attachment of biomolecules on surfaces modified with carboxy-terminated silane after their conversion to N-hydroxy succinimido-esters.

Please cite this article as: Makarona, E., et al., Point-of-Need bioanalytics based on planar optical interferometry, Biotechnol Adv (2016), http://dx.doi.org/10.1016/j.biotechadv.2016.02.005

The photon count P_c is limited by the number of spectrometer channels in the emission band and the vertical resolution of the digital spectrometer. In fact

$$P_c = M \times 2^{VR} \tag{18}$$

where M is the number of channels and the vertical resolution. Based on Eq. (16) the detection limit in terms of the minimum detectable biomolecular thickness is given by:

$$DL = \frac{3\delta t}{\pi L\left[\left(\delta N_s/\lambda\right)_a\right]\sqrt{P_c}} \tag{19}$$

In Eq. (19) δt is the biomolecular adlayer thickness which causes the $\delta N_s/\lambda$ increase in the N_s/λ ratio and $(\delta N_s/\lambda)_a$ is the average value of $\delta N_s/\lambda$ in the waveguided spectral band. According to Eq. (19) for a given spectrometer the LOD can decrease indefinitely by increasing the sensing arm length L. In practical terms, though, a lower limit on DL is placed by non-specific interactions and temperature fluctuations (White and Fan, 2008). In practical terms taking into account all possible noise sources, LODs of 1.35×10^{-6} (TE, $L_{sens} = 600$ μm), 7.4×10^{-7} (TE, $L_{sens} = 2$ mm), 5.8×10^{-7} (TM, $L_{sens} = 600$ μm) and 3.1×10^{-7} have been predicted (TM, $L_{sens} = 2$ mm). However, detection limits in the pm thickness range are achievable. Evaluation with water-isopropanol solutions yielded phase sensitivities at $S = 1958$ RIU^{-1} for TE and 4710 rad/RIU for TM. The LODs determined experimentally ($L_{sens} =$ 2 mm) were 2.75 × 10–^{6} RIU for TE and 4.58×10^{-6} RIU for TM.

When applied to closer-to-life scenarios, and in the direction of food safety and food adulteration detection schemes, the semi-integrated BB-MZI managed to detect 0.04% (v/v) bovine milk in goat milk with a dynamic range that varied between 0.1 and 1.0% (v/v). The results were comparable to ELISA developed using the same monoclonal antibodies, with the added benefit of providing answers within 10 min instead of 2 h that the corresponding ELISA lasted (Angelopoulou et al., 2015).

2.3.2. Multi-wavelength Young interferometry

In addition to BB-MZIs, a new approach to YI has been suggested (Mulder et al., 2012). Instead of using a single-wavelength source, the authors proposed of using three distinct wavelengths, as an expansion to the dual-wavelength scheme suggested by Stamm et al. (1998) or the dual-wavelength/polarization approach of Nellen and Lukosz (1993). From another point of view, the 3-wavelength YI could be seen as the counterpart of the BB-MZI.

The main idea behind the suggested MW-YI is that for each wavelength the penetration depth of the evanescent field is modified according to Eq. (2) being smaller for shorter wavelengths and more expanded for longer ones. Therefore, each wavelength probes the sensor surface to different depths allowing for discrimination between short molecules (such as proteins which are in the order of 5–10 nm) and bulk RI changes or larger particles (such as viruses with diameters of 50–200 nm). Assuming M adlayers building over the sensor surface and using K wavelengths at the input, the well-known relation between the phase and the effective refractive index changes has to be written in a matrix format as:

$$\Delta\varphi = M_s \cdot \Delta n \tag{20}$$

where $\Delta\varphi$ is an M × 1 matrix and Δn is a K × 1 matrix, with M_s the sensitivity matrix each element of which is expressed as:

$$M_{ij} = \frac{2\pi L}{\lambda_j} \cdot \frac{\partial N_{eff}}{\partial n_i} \quad , \quad i \in [1, M] \text{ and } j \in [1, K] \tag{21}$$

with $S_{ij} = \left(\partial N_{eff} \Big/ \partial n_i\right)_j$ the sensitivity coefficient of the ith layer for the jth wavelength. Any effective refractive index change in the ith layer can be determined with a precision that depends on the precision with which $\Delta\varphi_j$ can be measured defined by external factors such as laser noise, camera noise, and temperature fluctuations. A critical point that one should take into account when designing the MW-YI is that the three wavelengths should be considerably different in order for the mode profiles (and hence the evanescent filed penetration depths or else phrased the sensitivity coefficients) to be distinctly different and for M_s to be as less singular.

The authors performed simulations for several waveguide materials routinely used in IO sensors, such as Si_3N_4, Al_2O_3, and TiO_2 in order to define the optimum core thickness for each material for input wavelengths $\lambda_1 = 400$ nm, $\lambda_2 = 550$ nm, and $\lambda_3 = 700$ nm. Following the analysis, it is estimated that a LOD of the order of $\Delta N_{eff,min}$ in the order of 10^{-6} is anticipated for the MW-YI. Although this LOD is comparable to MZI or even better by at least one order of magnitude compared to SW-YI, it is expected to offer the advantage of distinguishing among specific binding, non-specific binding, and bulk RI changes. No actual implementation of the suggested scheme has been so far realized, and it will be very interesting if in the near future the anticipated performance can be tested in real-life settings for the analysis of real samples.

2.4. Other types of interferometric sensors

As it was mentioned above the standard interferometric implementations of planar waveguides are the single wavelength Mach–Zehnder and Young ones. In both implementations, the monochromatic light should be coupled into the waveguide and then the light is split into the sensing and reference arms. From the operation point of view the difference between them that the interference occurs on the chip in the MZI and on a CCD in the case of YI.

Recently a new concept of interferometry was introduced by L. Lechuga and her co-workers (Zinoviev et al., 2011; Duval et al., 2012; Dante et al., 2015) where the interference occurs between two waveguide modes of the same polarization (BiModal Waveguides, BiMW). The implementation of the particular concept relies again on the use of standard microelectronic/micromachining processes and offers the characteristic of the absence of any Y-shaped splitters which are standard parts of both MZI and YI.

2.4.1. Theory of bi-modal interferometry

In the BiMW structure, the interference happens between the fundamental and first-order modes both of them propagating in the same straight waveguide (Zinoviev et al., 2011; Duval et al., 2012). In the BiMW structure, monochromatic light from an external stabilized coherent source is coupled into a planar ridge waveguide which supports a single transversal mode; the fundamental mode. After a certain distance, the planar waveguide is shaped to be able to accommodate the propagation of two transversal modes. Therefore at this point, the fundamental mode that is propagating into the waveguide splits into two modes: the fundamental mode and the first order one. Then these two modes are propagating within the planar waveguide till the end of the silicon chip and an interference pattern is formed. In this interference pattern, the light intensity distribution depends on the optical properties of the layers involved in the structure. This interference pattern is recorded by an external two-section photodetector aligned against the chip.

For propagation of the light over the sensing area length (L), the phase difference between the two modes is given by:

$$\Delta\varphi(\lambda, n) = \frac{2\pi L}{\lambda}\left[N_1(\lambda, n) - N_0(\lambda, n)\right] = \frac{2\pi L \Delta N_{eff}(\lambda, n)}{\lambda} \tag{22}$$

where N_0 and N_1 are the effective refractive indices of the two propagating modes, respectively, ΔN_{eff} their difference, L the sensing area length and λ the wavelength of the light coupled in the chip. In the case of BiMW, the propagation of the two modes results in an output signal

that depends on the phase difference which is recorded by the two-section photodetector and is:

$$S_R = \frac{I_{up} - I_{down}}{I_{up} + I_{down}} \propto V\cos(\Delta\varphi) \quad (23)$$

where I_{up} and I_{down} are the currents measured in the two sections of the photodiode and V is the so-called visibility factor (0.5–0.7). S_R is normalized to the total optical power propagating in the BiMW structure, it is immune to fluctuations caused by laser or mechanical instabilities, preventing this way false-positive responses.

2.4.2. Bi-modal interferometry implementation

As in all other interferometric chips discusses so far, the BiMW chips are fabricated with mainstream microelectronic/micromachining processes applied on a Si wafer. The process flowchart starts with a thermally grown SiO_2 layer which acts as the bottom cladding layer of the waveguide followed by the deposition of a 350 nm thick Si_3N_4 layer which will act after appropriate patterning as the waveguide. Then the silicon nitride layer is shaped as a ridge type waveguides with a nominal width of 3 μm and ridge height of 2 nm through standard photolithography followed by BHF etching to allow for precise and repeatable control of the ridge height.

The section of the device that supports single mode operation has waveguide thickness of 150 nm to meet the simulations and theoretical calculations according to which the thickness should be less than 160 nm. After the patterning of the silicon nitride layer and the definition of the parts supporting the single and the two modes the wafer is covered by a SiO_2 top cladding layer. The last processing step is the opening of the sensing area in the top cladding layer through standard lithography and wet etching. The sensing area's length is 15 mm and is the half of the sensing chip's length. By applying the BiMW transduction principle, it is possible to accommodate 16 interferometers on a chip size of 30×10 mm^2. After the dicing, the emission edges of the chips are polished to achieve the appropriate optical quality end coupling.

The measurement set-up from the light coupling-in side is quite standard and employs a standard stabilized linearly polarized 632.8 nm laser the output of which is coupled into the waveguide through a microscope objective lens (40×). At the emission side of the chip, the interference pattern is monitored by a two sectional photodiode with each section connected to a current amplifier. For the operation, the chips should be placed on a thermally stabilized base with an accuracy of 0.01 °C.

The BiMW concept has been applied both for sensing of the bulk refractive index and for the real-time monitoring of bioreactions. The evaluation of the detection capabilities in term of bulk refractive index changes was based on HCl solutions covering a wide concentration range. The LOD, defined as three times of standard deviation of the signal at the baseline, was evaluated at 2.5×10^{-7} RIU (Zinoviev et al., 2011), while when an optical modulation format was introduced with a compact laser diode – in order to move towards a lab-on-chip application – a similar LOD of 3.3×10^{-7} RIU was achieved (Duval et al., 2012). These values are in the same range with the standard planar interferometric transducers.

In terms of biomarker measurements, the BiMW concept has been successfully implemented for the monitoring of immunoreaction between the C-reactive protein (CRP) and its monoclonal antibody (C7 antibody), previously immobilized on the sensor chip surface. From the calibration curve, which appears to be linear in terms of Δφ over CRP concentration, the LOD is estimated as 7 ng/ml; corresponding to a response equal to three times the baseline noise (Zinoviev et al., 2011). Correspondingly, the more compact version of the bi-modal interferometer of Duval et al. (2012) was capable of detecting down to 20 pM of hTSH (human thyroid stimulating hormone) following a competitive assay format. This LOD value is comparable to the value reached by more complicated assays and other transduction principles.

3. Surface functionalization

The intensive research for the realization of transduction principles offering low LODs comes in parallel with thorough research on the surface functionalization of the planar interferometers. As it was discussed in the previous section, the detection of biomolecules with optical sensors relying on refractive index changes is facilitated by the fact that biomolecules have higher refractive than both the air and the water. This means that the presence of biomolecules in the vicinity of the waveguide surface, i.e., within the penetration width of the evanescent wave, can affect the propagation of electromagnetic fields providing a mean for the detection of biomolecules. Nevertheless, to be able to detect a specific biomolecule quantitatively from a sample that could contain an enormous number of different molecules as usually are the biological, environment or food samples it is necessary to employ a strategy to immobilize an appropriate recognition element on the transducer surface and a strategy to avoid any other non-desirable interaction of the waveguided light with the matrix of the sample. The first requirement, i.e., the specificity of the binding is fulfilled by the careful selection of recognition element that depending on the targeted analyte could be an antibody, an oligonucleotide, a receptor or receptor binding molecule, a molecularly imprinted polymer, an aptamer and so on. These recognition elements should be immobilized on the transducer surface in a way that accomplishes the highest possible binding capacity but also repeatability from measurement to measurement and from sensor to sensor, stability under the conditions of measurements (e.g., under a constant flow rate and/or in complex matrices) or storage. Despite the high significance of bio-functionalization with respect to final system performance, there is a lack of systematic studies of how the different bio-functionalization approaches affect this performance as well as of data about the chemical characterization of bio-functionalized sensors. In addition, to the immobilization of recognition element in a functional form the efficient elimination of non-specific binding is also of paramount importance for the performance of the sensors in real applications were the matrix could vary from sample to sample and affect in a non-expectable manner the biosensing layer. Thus apart from referring to most common approaches for efficient immobilization of the recognition elements the approaches employed for suppression of non-specific binding will be also reviewed in the following sections.

3.1. Surface bio-functionalization approaches

The approaches employed for the attachment of recognition elements onto the sensing areas of the waveguiding structures (Mach–Zehnder, Young, Bi-modal interferometers, etc.) is mainly governed by the sensor material. The materials that have been used so far to construct integrated interferometers for biosensing applications are mainly silicon oxide, silicon nitride, silicon on insulator (SOI) and less often glass substrates, Ta_2O_5 or polymers. Glass substrates and Ta_2O_5 is usually the material of choice when gratings made on the same substrate are used for the coupling of light onto the waveguide. Nevertheless, the bio-functionalization approaches followed for these two materials do not differ so much from the respective for silicon based sensors. The procedure followed is in general completed in three steps that include cleaning/hydrophilization of the surface, chemical modification usually with a silane that offers the required surface wetting properties or moieties for coupling of recognition elements and finally attachment of recognition elements.

3.1.1. Surface cleaning approaches

For silicon-based sensors, the most commonly employed technique for surface cleaning is treatment in oxygen plasma, the particular conditions employed not always mentioned (Brosinger et al., 1997; Schipper

Please cite this article as: Makarona, E., et al., Point-of-Need bioanalytics based on planar optical interferometry, Biotechnol Adv (2016), http://dx.doi.org/10.1016/j.biotechadv.2016.02.005

et al., 1997a, 1997b; Weisser et al., 1999; Liu et al., 2013; Misiakos et al., 2014b). Another cleaning approach is based on the use of Piranha solutions, prepared by mixing concentrated sulfuric acid (H_2SO_4) with a 30% (v/v) hydrogen peroxide solution (H_2O_2) at 1:1, 2:1 (Drapp et al., 1997) or 3:1 ratio (Sarkar et al., 2014). In general, the ratio of concentrated sulphuric acid to hydrogen peroxide solution can vary from 3:1 to 7:3 and the treatment can be performed either at room temperature or under heating for times ranging from a few minutes to one hour. Treatment with nitric acid (Heideman et al., 1993; Densmore et al., 2009), heated sulphuric–chromic acid solution (Schneider et al., 1997, 2000a, 2000b), acetone (Hong et al., 2009), 3:1 25% NH_3:30% H_2O_2 (Schmitt et al., 2007) or commercially available cleaning solutions like Hellmanex (Hoffmann et al., 2007) or Micro-90 solution (Xu et al., 2007), are some of the methods that have been applied. Combinations of more than one methods or solutions have been also reported, the combinations extending from treatment with ethanol and nitric acid (Densmore et al., 2008), NaOH solution and oxygen plasma (Ma et al., 2015), Piranha and NaOH solution (Brandenburg et al., 2000). In addition to silicon- or tantalum-based sensors, oxygen plasma treatment has been applied to clean waveguides made of polyimide (Melnik et al., 2011). This report is one of the few where data about the cleaning method optimization are provided based on contact angle measurements, fluorescence intensity measurements and surface characterization by XPS.

All the above-mentioned treatments aim not only to remove organic material residues or other contamination from the sensors surface prior to the attachment of the particular recognition element, but also to enrich the surface with hydroxyl groups through which the attachment of silanes usually employed for sensor surface modification is achieved. It should be noted that in the case of devices, where apart from the waveguides, passive electrical components, like contact pads are integrated on the device, oxygen plasma treatment is the only viable solution since either strongly acidic or basic solutions are going to destroy these features (Misiakos et al., 2014a).

3.1.2. Chemical surface modifications

The chemical modification of the sensor surface depends on the strategy that will be followed by the recognition element attachment. In other words, the basic criterion for selection of sensor chemical modification approach is whereas the attachment of recognition molecules will be based on physical adsorption or covalent bonding which in turn is dictated by the nature of the recognition element. Thus, if the recognition element is a protein (e.g., an antibody) immobilization can be performed both via physical adsorption or covalent bonding. On the other hand, for small molecular weight molecules covalent bonding is the only alternative route. For charged molecules like oligonucleotides, adsorption governed mainly from ionic interactions is possible with the covalent attachment to prevail in most cases. Thus, the surface chemical modification approach applied should provide the functionalities required without affecting the optical properties of the sensor. Additional advantages are the simplicity of the procedure (few reaction steps, easy to find materials, biocompatible conditions), the reproducibility and the large-scale applicability.

3.1.2.1. Chemical surface modification by self-assembled silanes. The formation of a self-assembled silane layer is the most popular chemical modification method employed in optical sensors. It is based on the use of organofunctional alkoxysilanes which form covalent bonds with the sensor surface through condensation of siloxane groups on the silane molecules with the hydroxyl groups which have been created on the sensor surface through the cleaning/hydrophilization method (as discussed above) or are part of native silicon oxide layer always present on the silicon surfaces (Fig. 2b). Ideally, the chemical modification procedure should lead to a smooth and homogeneous silane monolayer with a thickness of approximately 1 nm (Awsiuk et al., 2012; Awsiuk et al., 2013a, 2013b). Although the mechanism of the silane layer formation seems to be straightforward it is actually complex enough and requires careful selection of conditions to obtain a layer with the desirable characteristics, especially when silanes with side functional groups intended for covalent bonding of recognition elements are implemented. Parameters like the solvent used (water or anhydrous organic solvents), the silane content, the duration and the temperature of the treatment could affect the final layer (Banuls et al., 2013). Nevertheless, the literature study reveals that in most cases these parameters are selected rather randomly or based on experience from planar glass or silicon surfaces and the formation of a silane monolayer is based mostly on belief rather that experimental proof. The methods applied for chemical modification of silicon-based interferometric sensors are grouped below on the basis of the terminal functionality of the organosilane employed.

3.1.2.1.1. Hydrophobic silanes. One of the first chemical modification approaches employed for interferometric sensors involved the use of silanes that could render the surface hydrophobic in order to immobilize protein molecules by physical adsorption. Thus, hexamethyldisilane (HMDS) (Heideman et al., 1993) or dichlorodimethylsilane (Schipper et al., 1997b) was applied on Mach–Zehnder made of silicon nitride after cleaning with nitric acid and oxygen plasma, respectively, to facilitate the physical adsorption of an antibody against human chorionic gonadotropin (hCG) or an atrazine conjugate with bovine serum albumin, respectively.

3.1.2.1.2. Amine-terminated silanes. Modification of silicon sensors via amine-organosilanes, and most particularly 3-aminopropyltriethoxysilane (APTES), is the most popular method used. The application of such a silane aims to the introduction of reactive amine groups onto the surface that could be then used for the coupling of the recognition elements. The creation of amine-organosilane layer usually employs treatment with the silane solution followed by thermal curing in order to stabilize the silane layer through the promotion of the condensation reaction with the surface hydroxyl groups. The conditions of both the silane deposition and curing vary greatly from one report to another. Thus, modification with APTES has been performed using 0.1% solution in dry toluene for 1 h followed by heating at 110 °C for 2 h (Brosinger et al., 1997), 10% aqueous solution, pH 3.45, at 80 °C for 2 h and curing at 100 °C for 1 h (Brandenburg et al., 2000; Jiang et al., 2014), 2% solution in a mixture of 95%/5% (v/v) ethanol/H_2O for 2 h and heating at 120 °C for 15 min (Liu et al., 2013; Liu et al., 2014; Liu et al., 2015), 10% solution in ethanol and drying at room temperature for 2 h (Choo et al., 2014), or 0.5% aqueous solution for 2 min and curing at 120 °C for 20 min (Misiakos et al., 2014a; Angelopoulou et al., 2015). APTES has been also deposited from vapors in a vacuum chamber (Densmore et al., 2008, 2009). Generally, the presence of water in the APTES (or in any other triethoxysilane) solution is recommended, since it promotes the reaction of less reactive, as compared to methoxy, ethoxy groups for interaction with the surface hydroxyl groups (Banuls et al., 2013). This is critical for the properties of the resulting silane layer since if there is no orientation and interaction of the silane ethoxy groups with the hydroxyl groups of the surface then they can form hydrogen bonds with the amine groups of the silane, resulting in a layer with sub-optimal reactive amine groups on its surface. Apart from APTES, 4-aminobutyldimethylethoxysilane (ABDMS) has been used for the modification of a Mach–Zehnder interferometer fabricated on a glass substrate (Drapp et al., 1997) following a procedure developed for a reflectometric interference spectroscopy sensor (Piehler et al., 1996) while treatment with N-[3-(trimethoxysilyl)propyl]-ethylene diamine has been employed for the modification of a Mach–Zehnder interferometer fabricated on a silicon oxide substrate (Hong et al., 2009).

3.1.2.1.3. Epoxy-terminated silanes. Epoxy-organosilanes, and especially 3-glycidoxypropyltrimethoxy-silane (GOPTS), have been also applied for the chemical modification of interferometric sensors. Thus, GOPTS has been employed by Schneider et al. (1997, 2000a, 2000b) to functionalize the sensing region of a Hartmann interferometer made of silicon nitride through overnight treatment with a 3% (v/v) GOPTS solution acidified to pH 2 with 1 M sulfuric acid, whereas the reference

Please cite this article as: Makarona, E., et al., Point-of-Need bioanalytics based on planar optical interferometry, Biotechnol Adv (2016), http://dx.doi.org/10.1016/j.biotechadv.2016.02.005

region was modified with a non-reactive silane (tridecafluoro-1,1,2,2-tetrahydo-octyl)-1-dimethylchlorosilane). GOPTS has been also applied to modify Young interferometers made of Ta_2O_5 by immersion in a 10 mM GOPTS solution in absolute toluene (in the presence of triethylene amine as a catalyst) for 48 h followed by curing at 120 °C for 4 h (Schmitt et al., 2007; Hoffmann et al., 2007). In contrast to APTES deposition, anhydrous organic solvents are recommended for GOPTS.

3.1.2.1.4. Thiol-terminated silanes. Thiol-terminated or mercapto-organosilanes is another category of functional organo-silanes that has found application in the chemical modification of interferometric sensors. The reagent almost exclusively used for this purpose is 3-mercaptopropyltrimethoxysilane (MPTMS), the conditions used for the modification, however, differ between reports. Thus, immersion in a 10% (v/v) MPTMS solution in toluene at room temperature for 12 h (Sepulveda et al., 2006) or 2% MTS solution in anhydrous toluene for 1 h (Xu et al., 2007) has been applied for the modification of silicon-based interferometers whereas immersion in a 3% (v/v) MPTMS solution in 0.07 M acetate buffer, 25% (v/v) methanol and 2.8% (v/v) Triton X-100 at room temperature for 1 h (Bruck et al., 2011; Melnik et al., 2011) has been applied for the modification of interferometer made of polyimide. Mercapto-methyl-dimethylethoxysilane has been also employed to modify a Mach–Zehnder made of silicon oxynitride (Busse et al., 1999) with the difference that the surface was not then used to immobilize some recognition element through reaction with the introduced thiol groups but for the deposition of a gold layer on which thiolated-molecules where then attached.

3.1.2.1.5. Carboxy-terminated silanes. Carboxy-terminated silanes and especially carboxyethyl-silanetriol have been applied successfully for the chemical functionalization of Bimodal Mach–Zehnder made of silicon nitride (Duval et al., 2012; Dante et al., 2012, 2015). One of the advantages of this modification method is that the silane deposition is performed from aqueous solutions avoiding any organic solvents. A process that also lead to the introduction of carboxyl groups onto the surface is that reported by Schlatter et al. (1993) according to which the interferometer surface is first modified by a layer of octenyl-trichlorosilane which is then subjected to oxidation using a mixture of $NaIO_4$ and $KMnO_4$ to create carboxyl groups onto the surface following a multi-step and rather cumbersome procedure.

3.1.2.1.6. Other silane-based chemical modification methods. The deposition of a dimethyl-monomethoxy-silane bearing a biotin moiety from a mixture with a carboxy-ended dimethylo-monomethoxy-silane has been reported (Weisser et al., 1999) as a mean to directly introduce on the surface of the sensing area of the MZI structure biotin groups to couple streptavidin. Due to lack of experimental data about exact modification conditions and yield in terms of biotin groups per surface area, it is difficult to evaluate the outcome of this approach.

3.1.2.2. Other surface chemical modifications. Although the employment of silane surface modification is considered unavoidable, especially for devices fabricated on silicon-based substrates, other chemical activation strategies are also possible. Thus, Sarkar et al. (2014) took advantage of the amine groups created on the silicon nitride surface by HF treatment to bind the bi-functional glutaraldehyde molecules leading to the introduction of amine-reactive aldehyde groups. Non-silane based surface chemical modification procedure can be also suitable for polymer based interferometric sensor. In this context, a poly(acrylic) acid layer has been created on the surface of a Mach-Zehnder made of SU-8 by plasma-induced graft copolymerization of acrylic acid monomer providing carboxyl groups for biomolecules attachment (Shew et al., 2008).

3.1.3. Recognition element attachment

The recognition element attachment strategies on the chemically functionalized surfaces of the reported interferometric sensors can be distinguished into two main categories, those relying on physical absorption and those based on some scheme of covalent bonding.

3.1.3.1. Physical adsorption. Physical adsorption relies mainly on Van der Walls interactions (interactions between induced, permanent or transient electric dipoles) between the surface and the molecules (mainly proteins), which although weak in nature can lead to very strong and irreversible attachment of these molecules on the surface. The advantages of this approach are mainly its simplicity, repeatability of the results ensuing optimization of the deposition conditions, and relative stability of immobilized molecules to flow conditions. As main disadvantage is considered the fact that the orientation of the biomolecules is rather random and thus a high percentage of immobilized molecules are not functional. Nevertheless, physical adsorption has been applied and is still applied to immobilize recognition molecules to optical sensors including the interferometric ones and it is the approach favoured by our group since the data we have received by comparison methods performed in our integrated BB-MZI devices showed that physical adsorption can perform equally well with covalent bonding even when extensive regenerations and continuous operation for days is required (Angelopoulou et al., 2015). To apply physical adsorption as recognition molecule immobilization strategy on silicon-based devices one can use the devices as they are (Heideman et al., 1991; Schipper et al., 1997a; Prieto et al., 2003; Ymeti et al., 2005, 2007; Gao et al., 2011; Zinoviev et al., 2011) or after modification with either a hydrophobic silane such as hexamethyldisilane (Heideman et al., 1993) or dichlorodimethylsilane (Schipper et al., 1997b) or a hydrophilic one like APTES (Brandenburg et al., 2000; Densmore et al., 2009; Misiakos et al., 2014a; Angelopoulou et al., 2015). Depending on the targeted analyte and the assay configuration implemented, the immobilized proteins in these reports are antigens (bovine serum albumin, immunoglobulins, pesticide-protein conjugates, casein, etc.) or antibodies against human or animal immunoglobulins, human plasma proteins, viruses, etc. Physical adsorption is also a straightforward procedure when the waveguides are made of polymers (Dér et al., 2010) since most of them have the capability to adsorb proteins irreversibly.

3.1.3.2. Covalent bonding. Covalent bonding has also its supporters, since the covalently bound molecules are considered more stable under flow conditions or when regenerations are desirable. They also considered more reproducible than physical adsorption and they can be tailored to provide for oriented immobilization which is expected to help in the preservation of immobilized molecules functionality, especially when antibodies or other binding proteins are considered. The chemistry applied in each case depends on the chemical activation of the sensor surface applied and of course the available reactive groups on the biomolecule.

On sensor surfaces that have been modified with amine-terminated organosilanes, molecules can be bound trough activation of their carboxy-groups with carbodiimide (e.g., EDC), N-hydroxysuccinimide (NHS), or a combination of these two reagents (Fig. 2). Thus, an activated NHS-ester of biotin has been immobilized directly on the sensors surface and used to monitor the specific binding of streptavidin (Densmore et al., 2008; Hong et al., 2006; Liu et al., 2013, 2014). Similarly, a single-stranded DNA sequence modified with an amine-end group has been also coupled to an APTES-modified Mach–Zehnder to monitor hybridization with a complimentary sequence. Aminosilane-modified surfaces can be also activated through bi-functional reagents like glutaraldehyde. This modification leads to a surface with reactive aldehydes which readily react with amine groups to form imines (Schiff bases) which are then converted to the more stable amine bonds by a sodium cyanoborohydride reduction step. Thus the immobilization of streptavidin (Kozma et al., 2011), goat IgG (Jiang et al., 2014) or an amine-terminated DNA sequence (Liu et al., 2015) has been reported. Other chemistries are also possible, for example the surface amine groups can be converted to carboxyl-groups though reaction with succinic anhydride, activated by EDC/NHS and then used for coupling of amine-bearing molecules (Drapp et al., 1997) or activated through reaction with cyanuric chloride and

Please cite this article as: Makarona, E., et al., Point-of-Need bioanalytics based on planar optical interferometry, Biotechnol Adv (2016), http://dx.doi.org/10.1016/j.biotechadv.2016.02.005

tribenzylamine to allow coupling of protein molecules (Brosinger et al., 1997).

The coupling of molecules on epoxy-silane modified sensor surfaces can be accomplished directly through reaction with their amine or sulfhydryl groups or after conversion of epoxy-groups to other functional moieties (Fig. 2d). Thus, Schneider et al. (1997, 2000a, 2000b) immobilized avidin, oligonucleotide probes, or antibodies against plasma protein or viruses on the sensing region of a Hartman interferometer modified with GOPTS after oxidation of epoxy groups with sodium periodate to create reactive aldehyde groups, which in turn react with amine groups on the protein molecules. GOPTS modified sensor surfaces have been also further reacted with bi-functional molecules such as ethylediamine (Schmitt et al., 2007; Hoffmann et al., 2007) or polymers like amino-dextran (Ma et al., 2015) to convert epoxy- to amine-groups and apply an amine-based chemistry for the immobilization of specific recognition molecule.

Concerning sensors modified with mercaptosilanes, coupling of recognition molecules can be performed through a thiol-group for the formation of a disulfide bond or an amine-group using a heterobifunctinal cross-linker that has a maleimido-group as thiol-reactive moiety (Fig. 2e). Although protein have thiol-groups, they are not available for reaction, and therefore the thiol–thiol interaction is usually applied for immobilization of small molecular weight molecules that bear thiol-groups like thiolated-oligonucleotides (Sepulveda et al., 2006). Due to the reversibility of the disulfide bond, sensors modified following this chemistry could be easily regenerated by treatment with a thiol-containing reagent such as dithiothreitol. To our knowledge, however, such a study has not performed yet. The thiol-maleimide reaction has been applied for the modification of interferometric sensors with biotin using commercially available maleimido-derivatives (Bruck et al., 2011; Melnik et al., 2011) or the coupling of antibodies using the heterobifunctional cross-linker maleimido-benzoyl-N-hydroxysuccinimide ester (Xu et al., 2007).

Finally, when a silane containing carboxyl groups has been employed for the modification of the sensor surface, conjugation is almost exclusively performed via reaction with available amine groups in the molecule to be immobilized (Fig. 2f). To accomplish this, the surface carboxyl groups are converted to active ester groups through reaction with an EDC/NHS mixture and then used to immobilize protein antigens (Dante et al., 2012; Duval et al., 2012) or antibodies (Dante et al., 2015) through stable peptide bonds. Care should be taken when this immobilization scheme is employed to avoid hydrolysis of active ester groups prior to the addition of the molecule to be immobilized. Although activation and coupling can be done in a single step, this is usually avoided due to the risk of formation protein–protein aggregates that can bind on to surface leading to non-repeatable results.

3.1.4. Biofunctionalization techniques

The chemical activation is usually performed in the whole area of the sensor. The deposition of the recognition element, however, might be desirable to be confined only to the sensing region. This is critical for interferometric sensors having windows on both the sensing and the reference arm, but it is also a desirable feature when multiple sensors are realized on a single chip aiming to multi-analyte determinations. For the first type of devices, specially designed cuvettes (Brandenburg et al., 2000) or flow cells (Dante et al., 2012) were employed in order to apply the recognition molecule only on the sensing channel, whereas the other one is modified by a non-reactive protein or filled with the reaction buffer during the monitoring of the binding reaction. Similarly, multi-fluidic channels have been used for specific functionalization of multiple sensors on a single chip with different recognition molecules (Duval et al., 2012). Robotic spotters have been also employed for the spatially selective deposition of different recognition molecules onto different sensors of the same chip (Densmore et al., 2009; Misiakos et al., 2014a; Angelopoulou et al., 2015); a procedure that it is also more easily adaptable to mass production and large-scale biofunctionalization.

In most cases the recognition elements are directly deposited (adsorbed or covalently bonded) onto the chemically activated surface of the interferometric sensors. Nevertheless, indirect immobilization schemes using specific binding molecules as a bridge between the surface and the actual recognition molecule have been also implemented. The concomitant advantage of these indirect immobilization schemes arises from the fact that the specific recognition element does not interacts directly with the surface. Thus, the effects on immobilized molecule functionality imposed either from structural changes do to physical adsorption or covalent binding are eliminated to great extent. The most popular indirect immobilization scheme is that based on the biotin-(strept)avidin system. The implementation of this scheme to interferometric sensors was realized by covalent attachment of biotin-moieties onto the sensor surface followed by sequential binding of streptavidin and biotinylated anti-analyte specific antibody (e.g., Hoffmann et al., 2007), or by direct coupling of avidin (Schneider et al., 1997; Schneider et al., 2000a) or streptavidin (Jiang et al., 2014) followed also by binding of biotinylated anti-analyte specific antibody. Another indirect coupling scheme is the one using bacterial proteins, protein A or protein G, which bind to the Fc fragment of immunoglobulins from different species. In interferometric sensors, protein A has been immobilized to the sensor surface and used to bind human IgG (Schlatter et al., 1993) or an anti-human serum albumin antibody (Ymeti et al., 2005). An interesting indirect immobilization approach has been proposed by Hong et al. (2009) for the biofunctionalization of a Mach-Zehnder device with a mouse monoclonal antibody against the C-reactive protein. This approach makes use of a calixcrown derivative which contains an aldehyde group for coupling on an amine-modified surface and a crown moiety that interacts with the hydrophobic residues of the antibody molecule.

3.2. Non-specific binding suppression approaches

The binding of molecules other than the targeted ones, i.e., the ones recognized specifically from the immobilized onto to the sensor recognition molecule, when a sample is run over the sensor surfaces can deteriorate the sensor sensitivity either by masking the specific reaction or by affecting the specific recognition element layer properties, e.g. by causing detachment of immobilized recognition element moieties. Therefore, it is critical to maintaining the non-specific binding as low as possible. This is usually achieved by employing a blocking step after the recognition element attachment onto the sensor surface. In general, when the immobilized recognition molecule is a protein (antibody; analyte-conjugate; protein A or G; avidin or streptavidin), the blocking agent is a non-reactive protein like bovine serum albumin (BSA). This agent is used at concentrations ranging from 0.1 to 1% (w/v) and the treatment of the surface can take from 0.5 h to overnight (Schlatter et al., 1993; Brosinger et al., 1997; Prieto et al., 2003; Hoffmann et al., 2007; Hong et al., 2009; Bruck et al., 2011; Melnik et al., 2011; Liu et al., 2013; Jiang et al., 2014; Misiakos et al., 2014a). Short chain hydrophilic polymers like poly(ethyleglycol) (PEG), which possess protein repellent properties have been also used as blocking agent on interferometric sensors (Schneider et al., 2000a, 2000b). Researchers have also employed commercial blocking buffers like SuperBlock® (Xu et al., 2007). Chemical blocking is also performed when the sensor surface has been chemically activated with an agent such as GOPTS that can readily react with a variety of functional groups. In these cases, ethanolamine (Sarkar et al., 2014; Duval et al., 2012; Dante et al., 2015) has been used to block the remaining free epoxy-groups after the recognition molecule attachment.

The effectiveness of the blocking agent depends strongly on the matrix of the sample to be analyzed. Thus, in our study concerning the determination of bovine k-casein in goat milk samples with the integrated BB-MZI sensor (Angelopoulou et al., 2015) we found

Please cite this article as: Makarona, E., et al., Point-of-Need bioanalytics based on planar optical interferometry, Biotechnol Adv (2016), http://dx.doi.org/10.1016/j.biotechadv.2016.02.005

Table 2
Performance of the planar interferometric sensors.

Publication	Type of materials	WG type	Wavelength of input source	L_{sens} (mm)	Minimum detectable amount	Sensitivity or LOD	Sensitivity or LOD per mm of sensing area length $\Delta N_{eff,min} \times L_{sens}$ or $\Gamma_{min} \times L_{sens}$ or $t_{ad,min} \times L_{sens}$
SW-MZIs							
Heideman et al. (1991)	Si_3N_4 waveguides with SiO_2 cladding layers	Slab; $t_{core} = 100$ nm	He–Ne laser $\lambda = 632.8$ nm	10 mm	Human chorionic gonadotropin: 25 nM	Drift: $\Delta\varphi_{drift}/\Delta t = 0.06\ \pi/h \rightarrow \Delta N_{eff,drift} = 2 \times 10^{-7}$ RIU minimum detectable phase shift:$\Delta\varphi_{min} = 0.6\ \pi$ corresponding to $\Delta N_{eff,min} = 1.9 \times 10^{-5}$ RIU	1.9×10^{-4} RIU mm
Heideman et al. (1993)	Si_3N_4 waveguides with SiO_2 cladding layers	Slab; $t_{core} = 100$ nm	He–Ne laser $\lambda = 632.8$ nm	10 mm	Human chorionic gonadotropin): 50 pM	Improved phase drift compared to Heideman RG, 1991 minimum detectable phase shift:$\Delta\varphi_{min} = 0.01\ \pi$ $\Delta N_{eff,min} = 6.33 \times 10^{-7}$ RIU	6.33×10^{-6} RIU mm
Heideman and Lambeck (1999)	Si_3N_4 and SiON waveguides with SiO_2 cladding layers optimized for TM rejection – electro-optic modulation to enhance performance	Rib; $w = 4\ \mu m$, $t_{core} = 70$ nm, $t_{rib} = 15$ nm	He–Ne laser $\lambda = 632.8$ nm	4 mm	Improvement of drift to $\Delta\varphi_{drift}/\Delta t = 1 \times 10^{-4} \times 2\pi/h$	Taking ×3 drift value as minimum detectable change $\Delta\varphi_{min} = \times 10^{-4} \times \pi$ corresponding to $\Delta N_{eff,min} = 4.75 \times 10^{-8}$ RIU	1.19×10^{-8} RIU mm
Brosinger et al. (1997)	SiON waveguides with SiO_2 cladding layers	Rib; $w = 2\ \mu m$, $t_{core} = 350$ nm, $t_{rib} = 55$ nm	He–Ne laser $\lambda = 632.8$ nm	12 mm	Refractometric sensing: water/ethanol solutions $\Delta n_{c,min} = 1.8 \times 10^{-5}$ RIU Affinity sensing: 1 μg/ml of 2,4-dichlorophenoxy-acetic acid	$\Delta\varphi/\Delta n_c = 2.64 \times 10^3\ \pi$/RIU $\Delta\varphi_{min} = \pi/20$ corresponding to $\Delta n_{c,min} = 1.8 \times 10^{-5}$ RIU N/A[a]	1.5×10^{-4} RIU mm N/A
Weisser et al. (1999)	SiON waveguides with SiO_2 cladding layers	Rib; $w = 2\ \mu m$, $t_{core} = 350$ nm, $t_{rib} = 55$ nm	He–Ne laser $\lambda = 632.8$ nm	12 mm	Refractometric sensing: NaCl aqueous solutions Affinity sensing: streptavidin (assuming $n_{ad} = 1.45$ and using SPR to calculate t_{ad}) $t_{ad} \approx 2.8$ nm ($\delta n_c = 3 \times 10^{-3}$) was detected	For 0.5 M NaCl ($\delta n_c = 5.1 \times 10^{-3}$) $\Delta\varphi = 11.7\pi$ $\Delta\varphi_{min} = \pi/20$ ($\Delta N_{eff,min} =$ $\Delta\varphi/\Delta n_c = 2.3 \times 10^3\ \pi$/RIU $t_{ad} \approx 2.8$ nm ($\delta n_c = 3 \times 10^{-3}$) was detected $\Delta\varphi/\Delta t_{ad} = 2.9\pi$/nm $t_{ad,min} = 20$ pm → $\Gamma = 2$ ng/cm^2	$t_{ad} \times L_{sens} = 33.6$ nm mm
Schipper et al. (1997)	Si_3N_4 waveguides with SiO_2 cladding layers	Rib; $w = 4\ \mu m$, $t_{core} =$ 100–200–400 nm (to test sensitivity vs t_{core}), $t_{rib} =$ 3 nm	He–Ne laser $\lambda = 632.8$ nm	5 mm	Refractometric sensing: water/glucose solutions $n_c = 1.3358$–1.3451 with δn_c steps of 9.5×10^{-3} Affinity sensing: human chorionic gonadotropin: 30 nM	$\Delta\varphi/\Delta n_c = 2.8 \times 10^3 \times \pi$/RIU drift < 0.5 π/h	N/A since $\Delta\varphi_{min}$ not provided)
Schubert et al. (1997)	SiON waveguides with SiO_2 cladding layers	Rib WGs	Solid-state $\lambda = 670$ nm	1 or 8 mm (to test effect of L_{sens} length)	Refractometric sensing: water/glycerol solutions $n_c = 1.333$–1.38 with δn_c steps of 2×10^{-4} "food application": detection of water in cherry liqueur 1 g/100 ml	N/A	N/A
Prieto et al. (2003)	Si_3N_4 waveguides with SiO_2 cladding layers	1) ARROW $t_{core} = 3\ \mu m$, 39 nm overlay 2) ARROW $t_{core} = 3\ \mu m$, 37 nm overlay	He–Ne laser $\lambda = 632.8$ nm TE	1) 10 mm 2) 15 mm	1) Refractometric sensing: water/glucose solutions $n_c = 1.3325$–1.4004 2) Affinity sensing: HAS (human serum albumin)	1) $\Delta n_{c,min} = 2 \times 10^{-5}$ RIU → $\Delta N_{eff,min} = 4 \times 10^{-7}$ RIU 2) $t_{ad} = 1.8$ nm (7.7 μM)	1) 4×10^{-6} RIU mm 2) $t_{ad} \times L_{sens} = 27$ nm mm
Blanco et al. (2006)	Si_3N_4 waveguides with SiO^2 cladding layers	Rib; $w = 4\ \mu m$, $t_{core} = 200$ nm, $t_{rib} = 4$ nm	He–Ne laser $\lambda = 632.8$ nm TM	15 mm	Refractometric sensing: HCl aqueous solutions	$\Delta n_{c,min} = 3.8 \times 10^{-6}$ RIU → $\Delta N_{eff,min} = 2 \times 10^{-7}$ RIU[b] $\Delta\varphi/\Delta n_c = 1.184 \times 10^3\pi$/RIU	3×10^{-6} RIU mm
Dante et al. (2012)	Si_3N_4 waveguides with SiO_2 cladding layers	Rib; $w = 4\ \mu m$, $t_{core} =$	Commercial laser diode[c]	15 mm	Refractometric sensing: HCl aqueous solutions	$\Delta\varphi/\Delta n_c = 8.48 \times 10^3\ \pi$/RIU $\Delta\varphi_{min} = 0.0017$	2.85×10^{-6} RIU mm

		200 nm, t_{rib} = 1 nm	λ = 660 nm Tμ			corresponding to $\Delta N_{eff,min} = 1.9 \times 10^{-7}$ RIU	
Hiraoui et al. (2012)	SOI – porous silicon	ARROW; w = 4 μm	λ = 1.55 μm	5 mm	Feasibility study with ethanol drops	16 fringes corresponding to $\Delta n_c = 2.48 \times 10^{-3}$ RIU	N/A
Sarkar et al. (2014)	Si_3N_4 waveguides with SiO_2 cladding layers	Rib; w = 4 μm, t_{core} = 250 nm, t_{rib} = 4 nm	He–Ne laser λ = 632.8 nm	15 mm	*Listeria monocytogenes*	LOD: 10^5 CFU/ml Dynamic range: 10^5–10^{10} CFU/ml	N/A
Liu et al. (2014)	Si_3N_4 waveguides with SiO_2 cladding layers	Slot WG as sensing arm Strip WG as reference	Tunable laser λ = 1.56 μm TE	7 mm	Refractometric sensing: NaCl aqueous solutions Affinity sensing: streptavidin DAPK gene specific sequence (hybridization)	$\Delta\varphi/\Delta n_c = 1.864 \times 10^3$ π/RIU 95 nM → Δφ = 10.6π → Γ = 2.33 ng/mm^2 Mass sensitivity: 4.55 π/ngmm^{-2} $\Delta\varphi_{min} = 0.01 \rightarrow \Gamma_{min} = 2.2$ pg/mm^2 or $\Delta m_{min} = 35$ fg or $[M]_{min} = 18.9$ fM 1 nM (1 pmol/ml)	N/A $\Gamma_{min} \times L_{sens}$ = 1.63 pgmm^{-2} mm N/A
Liu et al. (2015)	Si_3N_4 waveguides with SiO_2 cladding layers	Slot WG as sensing arm Strip WG as reference[d]	Tunable laser λ = 1.56 μm TE	7 mm	L858R mutation in EGFR gene (epidermal growth factor receptor)	99:1 wild-type to mutate cells or 0.125 pg/ml	N/A (3 orders of magnitude lower than gel electrophoresis analysis of PCR products
Shew et al. (2008)	SU-8 based	Strip	NIR laser λ = 1.31 μm	3 cm	Affinity sensing: Rabbit IgG	1 ng/ml (ca. 6.7 × 10 pM)	N/A
Bruck et al. (2011)	Poyimide	Rib	NIR laser λ = 1.31 μm	1 cm	Affinity sensing: streptavidin	0.1 μg/ml (1.66 nM)	N/A
SW-YI							
Brandenburg (1997)	Borosilicate	Strip; w = 3 μm, t ~ 300–400 nm	λ = 790 nm	20 mm	Refractometric sensing: aqueous saccharose solutions	$\Delta N_{eff,min} = 5 \times 10^{-9}$ RIU	1×10^{-7} RIU mm
Brandenburg et al. (2000)	SiON waveguides with SiO_2 cladding layers	Strip; w = 3 μm, t = 400 nm	He–Ne laser λ = 632.8 nm	12 mm	Refractometric sensing: aqueous saccharose solutions Affinity sensing: IgG	$\Delta N_{eff,\ min} = 9 \times 10^{-8}$RIU 130 pM (50 ng/ml) Γ_{min} = 750 fg/mm^2	1.08×10^{-6}RIUmm $\Gamma_{min} \times L_{sens}$ = 9 pgmm^{-2}.mm
Hoffmann et al. (2007)	Glass substrate with Ta_2O_5 film (supplied by Unaxis Optics, Balzers)	Slab; t = 154 nm	Superluminescence diode λ = 675 nm	5 mm	Affinity sensing: NPT-tagged proteins	$\Delta N_{eff,\ min} = 9 \times 10^{-8}$ RIU 160 ng/ml (7.4 nM)	4.5×10^{-7} RIU mm
Schmitt et al. (2007)	Glass substrate with Ta_2O_5 film (supplied by Unaxis Optics, Balzers)	Slab; t = 154 nm	Superluminescence diode λ = 675 nm TM	5 mm	Refractometric measurements: glycerine dilutions Affinity sensing: IgG	$\Delta N_{eff,\ min} = 9 \times 10^{-9}$ RIU 270 pM	4.5×10^{-8} RIU mm
Ymeti et al. (2005)	Si_3N_4 waveguides with SiO_2 cladding layers	Rib; w = 2 μm, t_{core} ~ 90 nm, t_{rib} ~ 1 nm	Ar laser λ = 647 nm TE	4 mm	Affinity sensing: HSA	$\Delta N_{eff,\ min} = 6 \times 10^{-8}$RIU Γ_{min} = 20 fg/mm^2	4.8×10^{-7}RIUmm $\Gamma_{min} \times L_{sens}$ = 80 fgmm^{-2}.mm
Ymeti et al. (2007)	Si_3N_4 waveguides with SiO_2 cladding layers	Rib; w = 2 μm, t_{core} ~ 90 nm, t_{rib} ~ 1 nm	Ar laser λ = 647 nm TE	4 mm	herpes simplex virus type 1 (HSV-1)	850 particles/ml	N/A
BB-MZI							
Misiakos et al. (2014a)	Si_3N_4 waveguides with SiO_2 cladding layers	Rib; w = 1.25 μm, $t_{core,sens}$ = 162 nm, $t_{core,ref.}$ = 167 nm, t_{rib} = 5 nm	Si-avalanche diode broad-band spectrum: 500–900 nm both TE and TM	600 μm	Refractometric sensing: Water/isopropanol solutions Affinity sensing: anti-mouse IgG and streptavidin	$S\Phi = \Delta\varphi/\Delta n_c = 185$ πRIU^{-1} $\Delta N_{eff,\ min} = 1.09 \times 10^{-5}$ RIU 10 nM and 1 nM easily detectable in a multiplexed format	6×10^{-6} RIU mm
Misiakos et al. (2014b)	Si_3N_4 waveguides with SiO_2 cladding layers	Rib; w = 1.25 μm, $t_{core,sens}$ = 140 nm, $t_{core,ref.}$ = 167 nm, t_{rib} = 5 nm	Si-avalanche diode broad-band spectrum: 500 nm-900 nm both TE and TM	600 μm 2 mm	Refractometric sensing: WATER/isopropanol solutions $S_{TE} = \Delta\varphi/\Delta n_c = 0.624 \times 10^3 \times \pi$RIU^{-1} $S_{TM} = \Delta\varphi/\Delta n_c = 1.5 \times 10^3 \times \pi$RIU^{-1}	$\Delta N_{min,TE} = 1.35 \times 10^{-6}$ RIU $\Delta N_{min,TM} = 5.18 \times 10^{-7}$ RIU $\Delta N_{min,TE} = 7.4 \times 10^{-7}$ RIU $\Delta N_{min,TM} = 3.1 \times 10^{-7}$ RIU	8×10^{-7} RIU mm 3.11×10^{-7} RIU mm 1.48×10^{-6} RIU mm 6.2×10^{-7} RIU mm
Angelopoulou et al. (2015)	Si_3N_4 waveguides with SiO_2 cladding layers	Rib; w = 1.25 μm, t_{core} = 150–160 nm, t_{rib} = 5 nm	Si-avalanche diode broad-band spectrum: 500 nm-900 nm both TE and TM	600 μm	Detection of bovine milk in goat's milk Detection of k-casein in goat's milk	0.04% (v/v) 0.06 μg/ml	N/A
BB-YI							
Mulder et al. (2012)	Si_3N_4 or TiO_2 or Al_2O_3	Slab	400, 550 and 700 nm	N/A	Theoretical estimation	$\Delta N_{eff,\ min} = 10^{-6}$ RIU	~1×10^{-6} RIU mm

(continued on next page)

Please cite this article as: Makarona, E., et al., Point-of-Need bioanalytics based on planar optical interferometry, Biotechnol Adv (2016), http://dx.doi.org/10.1016/j.biotechadv.2016.02.005

Table 2 (*continued*)

Publication	Type of materials	WG type	Wavelength of input source	L_{sens} (mm)	Minimum detectable amount	Sensitivity or LOD	Sensitivity or LOD per mm of sensing area length $\Delta N_{eff,min} \times L_{sens}$ or $\Gamma_{min} \times L_{sens}$ or $t_{ad,min} \times L_{sens}$
Bi-modal							
Zinoviev et al. (2011)	Si-based bi-modal (Si_3N_4 waveguides with SiO_2 claddings)		He–Ne laser $\lambda = 632.8$ nm	15 mm	Refractometric sensing: HCl aqueous solutions Affinity sensing: anti-BSA antibody	$\Delta N_{eff,\,min} = 2.5 \times 10^{-7}$ 50 μg/ml[e]	3.75×10^{-6} RIU mm
Duval et al. (2012)	Si-based bi-modal (Si_3N_4 waveguides with SiO_2 claddings)		High-power laser diode $\lambda = 658$ nm	15 mm	Refractometric sensing: HCl aqueous solutions Affinity sensing: human thyroid stimulating hormone (competitive assay)	$\Delta N_{eff,\,min} = 3.3 \times 10^{-7}$ 20 pM	4.95×10^{-6} RIU mm

[a] N/A: non-applicable due to lack of pertinent information.
[b] By extrapolation of sensitivity curve assuming that the lowest detectable phase change is $0.1 \times 2\pi$ (as quoted by the authors).
[c] All-optical phase modulated MZI to solve phase ambiguity.
[d] Combined with isothermal solid-phase DNA amplification.
[e] One test as feasibility study – not the minimum detectable value.

that the best blocking agent was 100-times diluted goat milk. Other parameters that can affect the performance of a specific blocking agent are the fluidic layout, the flow rates and the buffers employed during the reaction. Despite the significance of an efficient blocking to the sensor performance, only a small amount of data about the effect of different blocking solutions on the same sensor analytical score are available.

3.3. Characterization of biofunctionalized sensors

The methods involved in the evaluation of the different chemical activation and bio-functionalization methods applied to interferometric sensors are the usually implemented surface characterization methods. These methods are applied either on planar surfaces of similar composition with that of the actual sensors or on the sensors themselves. Thus, the thickness of the layers formed is usually determined by ellipsometry, their wetting properties by water contact angle measurements, their chemical composition by FT-IR spectroscopy, XPS, and ToF-SIMS, and, their topography by AFM. The effectiveness of recognition or targeted molecule immobilization on a chemically activated surface has been also verified and/or quantified using molecules labeled either with radioisotopes (Schneider et al., 2000a) or fluorescent labels (Hong et al., 2009). The results obtained using radioisotope-labeled molecules are more easily quantifiable as compared to those using fluorescently-labeled ones due to the fact that fluorescence emission is highly affected by the label environment and silicon surfaces have been reported to have a quenching effect on fluorescent molecules emission (Bras et al., 2004). Nevertheless, labeling with fluorescent molecules is closer to the practices and expertise of most analytical labs than radiolabeling. Despite the availability of all these methods the data from the characterization of the sensor or sensor-like during or after the chemical activation and/or biofunctionalization are far from abundant or complete. To this end, our group has dedicated a lot of effort to characterize sensor surfaces after each step of the chemical activation/biofunctionalization procedure by applying a combination of surface characterization techniques and develop tools for acquisition of the maximum possible data from the respective measurements. Thus, combination of data obtained from angle-resolved XPS (ARXPS), AFM and ToF-SIMS (Awsiuk et al., 2012, 2013a, 2013b) allowed the calculation of layer thickness after each step, revealed the complex character of interactions between the immobilized IgG molecules with the blocking agent (BSA) and an anti-IgG antibody and suggested different immobilized proteins conformation on differently activated surfaces. The study which has mainly performed on planar silicon oxide and silicon nitride surface is now extending to BB-MZI chips functionalized with different recognition biomolecules.

4. Discussion

4.1. Comparison of the various interferometric techniques

In the previous sections, an overview of the various interferometric techniques along with various biofunctionalization strategies was presented in an effort to delve into the specifics of each approach, to describe its advantages and to pinpoint the inherent limitations. However, the variety of approaches and architectures pursued by every research group renders a direct comparison of the performance of the realized devices non-trivial. Therefore, it is necessary to introduce an "objective" metric in order to be able to compare the limits of detection of the various interferometric devices. In general, the LOD of a device was expressed as the minimum detectable change of the effective index of refraction ΔN_{min} *over the sensing area*. Another figure of merit that was employed in several cases was the minimum surface density Γ_{min} expressed in ng/mm^2 or the minimum detectable adlayer build up $t_{ad,min}$, which affect the effective refractive index and are interlinked with it. As discussed in Section 2, ΔN_{min} is inversely proportional to the sensing arm length, Eq. (2), meaning that devices with longer sensing arms would apparently provide lower LODs compared to devices with shorter sensing arms. Hence, a more objective way to evaluate and directly compare the performance of the sensors was to "normalize" the reported LODs *per mm of sensing arm length* either in terms of ΔN_{min} or in terms of Γ_{min} $t_{ad,\ min}$. The compiled effort towards this direction is presented in Table 2. Whenever the provided information was not enough for the corresponding calculations, the indication N/A (non-applicable) was denoted. In the same table useful information about a wide range of aspects is included and in particular for: type of waveguides used (materials and architecture), the wavelength of the input, the sensing arm length, the type of analysis performed, the minimum reported LODs and in the final column the normalization of the figures of merit per mm of sensing arm length whenever possible.

The normalized values of $\Delta N_{min} \times L_{sens}$ expressed in RIUmm have been plotted versus the year of publication for each of interferometric sensor (Fig. 3) principle of operation. When viewed from this perspective, it is worth noting that SW-MZI seems to have reached a plateau and most probably its limits. The BiMW has LODs in the same order of magnitude as the SW-MZI while from the BB-MZIs only the semi-integrated version seems able to lower the LOD by an order of magnitude. Surprisingly enough, even though not explored as intensively as the MZI, YIs have offered the lowest limits of detection from the very beginning, which are up to two orders of magnitude better than those reported for MZIs. In retrospect, it seems almost counter-intuitive that YIs have been less-favoured even though their performance has not only been rivaling, but surpassing that of MZI. In addition, the inherent MZI disadvantages of phase ambiguity and signal fading (that require modulation in order to be overcome), are not an issue in YI where a shifting interferogram is recorded. It has been argued that YIs have three major disadvantages (Kozma et al., 2014): (1) the fact that the final system has to be mechanically isolated, since the environmental noise and the ambient fluctuations may blur the interference fringes; (2) in case of multi-analyte detection with the multi-channel YI configuration (Ymeti et al., 2003), the precise adjustment of the end facet-image sensor distance is crucial; (3) the increased cost of the image detectors that can ensure high signal-to-noise ratio adds to the final cost of the system, rendering YI less attractive in terms of marketable PoN applications. As far as the first argument is concerned, the mechanical isolation does not only apply to YIs. MZIs and BiMWs require mechanical isolation of the system in order to keep all external components aligned to the interferometric chips and to minimize the environmental noise sources. Secondly, the precise adjustment of the end-facets is critical in all types of interferometric sensors, multi-channel or not, irrespective of the technique (Young, Mach–Zehnder or bi-modal). The only case that the end-facet is not an issue is in the case of the fully-integrated BB-MZI (Misiakos et al., 2014b), where the detector is monolithically integrated on-chip. Finally, the cost of high-performance CCDs cameras nowadays is not anymore prohibitive, while the size has also decreased. Moreover, the phase modulation of MZI or BiMW devices requires additional electronics that may increase the cost as well as the complexity of the final system rendering the cost argument against YIs obsolete. Therefore, it seems that YIs not only are at a disadvantageous position compared to MZIs, but they could be considered as the candidates to be reckoned with in the pursuit of ever increasing LODs and overall PoN system performance and cost-efficiency.

Nonetheless, irrespective of this effort to compile and compare the LODs of the several interferometric devices, one should not view the various reported methods as antagonists in a winner-takes-all competition. Nor should the provided comparison of LODs, serve as an elimination guide to exclude possible candidates as "non-fit" contestants for future PoN system. On the contrary, one of the scopes of this review was to identify the pros and cons of the various suggested interferometric approaches and to demonstrate that there is not a universal solution to all PoN applications.

Please cite this article as: Makarona, E., et al., Point-of-Need bioanalytics based on planar optical interferometry, Biotechnol Adv (2016), http://dx.doi.org/10.1016/j.biotechadv.2016.02.005

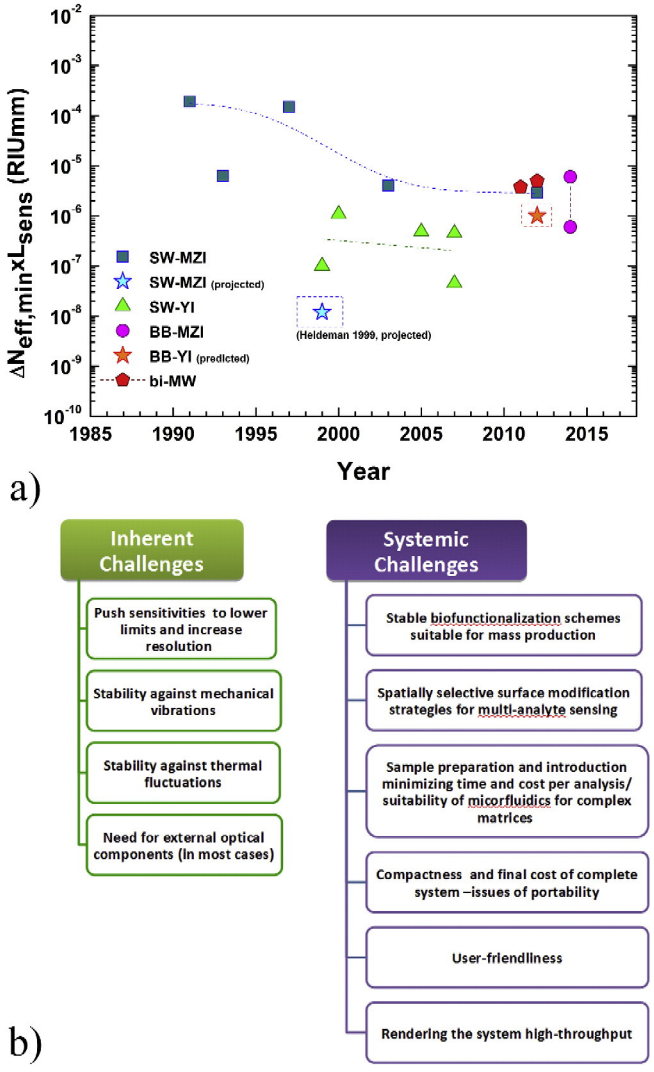

Fig. 3. Normalized LODs $\Delta N_{min}.L_{sens}$ per year of publication for each type of interferometric sensor [squares: SW-MZI; blue star: projected value from noise level considerations (Heideman and Lambeck, 1999); triangles: SW-YI; circles: BB-MZI; orange star: predicted value of BB-YI (Mulder et al., 2012); pentagons: Bi-MI]. Lines are solely used as guides to the eye.

4.2. Technological challenges and future trends

The evolution of interferometric sensors over the past twenty years has been indisputably impressive, opening up exciting opportunities for a large variety of applications especially in the direction of label-free PoN systems. Despite the tremendous potential that is lying in them, interferometric sensors have not yet managed to break free from the lab bench and find their way into marketable solutions for label-free PoN applications. The hurdles that have decelerated their evolvement into applicable systems are both "inherent" –in the sense that there exist limitations that emanate from the very nature of the sensors themselves- as well as "external" or otherwise termed "systemic" -in the sense that there exist technological challenges to circumvent into building a complete, compact, robust, reliable and at the same time user-friendly system irrespectively of how sensitive and reliable the sensor in itself is. This section is devoted to presenting both the "inherent" and the "systemic" challenges that interferometric sensors face into their struggle to be transformed to actual marketable systems for PoN applications. It is divided into three subsections, one devoted to the inherent challenges, a second focusing on the systemic challenges, and a final one about the possible routes and future trends of interferometric sensors. As a comprehensive overview, the challenges were summarized in the form of a schematic in Fig. 3b.

4.2.1. Inherent challenges of interferometric sensors

Considering first the inherent limitations of interferometric sensors, it is useful to recur to the graph of Fig. 3a. It appears that SW-MZI has been reaching its limits. Apart from the projected value of Heideman et al. (Heideman and Lambeck, 1999), which is based on the noise levels of a phase modulated MZI, there is a limit of 10^{-6} RIU mm that has not yet been surpassed. This limit seems to be imposed by the method itself and stems mostly from all external factors analyzed in Section 2, with the most prominent ones being the thermal fluctuations (which set a limiting factor on the length of the sensing area) and the mechanical vibrations that cause optical losses through the coupling of the interferometric chip with the external optical components. At the same time, BiMW seems to perform on an equal par with the best SW-MZI and are also limited to a LOD of 10^{-6} RIU mm. Nonetheless, there have been clear evidence that suitable photonic engineering, as in the case of slot-waveguide based SW-MZIs (Liu et al., 2015) can lead to impressive detection limits in closer-to-reality evaluation schemes (it is reminded that in the particular reference, 1:99 mutant-to-wild type cell was detected, a sensitivity that surpassed by 3 orders of magnitude gel electrophoresis analysis of PCR samples).

On the other hand, SW-YIs have exhibited a better performance compared to SW-MZI (up to two orders of magnitude) while it appears that they have not reached a limit yet. In one of the latest publications on SW-YIs, herpes simplex virus type 1 (HSV-1) was detected in an impressive concentration of 850 particles/ml (Ymeti et al., 2007). Still, the issues of thermal fluctuations and mechanical stability are open.

Interestingly enough, broad-band interferometry appears to be a very promising candidate for PoN applications, especially in the context of clinical applications where detection has to be performed in the complex media of bodily fluids. The interrogation of a broad spectrum along with the capability of dual-polarization detection significantly helps in discriminating among specific binding, non-specific interactions and bulk refractive index changes, opening up the way for new explorations. In all cases, though the issues of thermal and mechanical stability need to be met keeping in mind that PoN systems need to be transferrable and hence immune to movement. The only exception to this constraint appears to be the fully-integrated BB-MZI (Misiakos et al., 2014b) which contains all passive and active optical components on the same chip and has gotten rid of all external optical paraphernalia. Still, this great advantage is counter-balanced by lower sensitivity and a LOD one order of magnitude worse than SW- MZIs or the semi-integrated version.

Finally, an additional problem that is not entirely inherent, but also affects the sensor development on the system level, arises from the need to effectively control and stabilize the temperature. As already mentioned, temperature fluctuations affect the LOD and resolution of an interferometric sensor mostly by posing a limit to its length –which is directly related to its analytical capabilities. In general, the on-chip temperature fluctuations do not significantly add to the noise, since the two arms are closely placed within a few tens of microns. However, the temperature fluctuations may induce noise in the detectors, and more specifically in the case of YIs ambient fluctuations may blur the interferograms. Adding temperature-controlling modules definitely add to the size the weight and cost of the final system, and may also affect the operation complexity. Of course, there could be cases that the temperature-induced noise is within acceptable limits and is not prohibitive for the system operation and accuracy (e.g. when qualitative determinations are required or signaling that an analyte is over a predefined limit).

Up to now, there are no clear solutions that could contribute into circumventing these "self-imposed" limitations of interferometric sensing. The most realistic route seems for one to weigh the benefits of each approach, take into account the limitations and tailor the sensing method the requirements and specifications of the envisioned application.

Please cite this article as: Makarona, E., et al., Point-of-Need bioanalytics based on planar optical interferometry, Biotechnol Adv (2016), http://dx.doi.org/10.1016/j.biotechadv.2016.02.005

4.2.2. Systemic technological challenges

Moving from the inherent factors that have placed serious challenges to the development of interferometric sensors into viable products, one should take into account the external factors not related to the principle of operation per se, but are more related to the systemic approach.

One often overlooked factor is that of the bio-functionalization. Despite the availability of several chemical activation and biofunctionalization approaches, few of those have been already applied to interferometric sensors, as it has been reviewed in the previous sections; the issue of sensors surface modification and biofunctionalization procedures is still pending. There is, for example, still the need for new techniques that will allow for the coupling of recognition molecules in a manner that will preserve their functionalities will be accomplished in a few steps, and provide increased regeneration potential and stability of immobilized molecules. Promising approaches have been already applied to other optical sensors and might also work equally well for the interferometric ones. For example, DNA-directed antibody immobilization has been extensively applied to ring resonators (Kindt and Bailey, 2013) and click chemistry approaches for silicon surfaces have been developed (Caipa Campos et al., 2010) but not yet demonstrated on sensors. On the area of recognition molecules, the replacement of antibody or protein molecules from lower molecular weight synthetic analogs, such as peptide nucleic acids (PNA) and aptamers, have been already used in other sensing platforms with impressive results in some cases. The quest for robust and stable recognition molecules that will help to improve the analytical performance and expand self-life of sensors is only in its beginning. Little progress has been made also in the direction of efficient approaches for spatially selective immobilization of different recognition molecules on arrays of adjacent interferometric sensors for multi-analyte determinations. The so far employed microfluidic systems and robotic spotters have severe limitations with respect to the volume of the chips that could be processed in a reasonable time frame as well as the reproducibility of the biofunctionalization. To this direction, approaches compatible with the sensors fabrication techniques and applicable to wafer scale such as photolithographic ones could provide a viable solution.

Alongside the bio-functionalization issue, lies one other overlooked challenge, that of the sample preparation. This step hardly discussed in the publications has to be as simple as possible when one envisions a PoN system. Having a robust, compact, rapid, accurate and easy-to-use sensor is practically useless if the sample preparation is time-consuming, complex and has to be performed by highly-skilled personnel. In the most desirable scenarios simple processing steps like a dilution of the samples collected, hand mixing with appropriate buffers or even short centrifugation by a portable instrument should be enough. This entails, of course, a clearer understanding of fluid dynamics and the circulation of complex media within the microfluidic modules. For PoN devices, the ideal fluidic would not require external components like pumps to provide for fluid circulation over the sensors for time enough to get a measurable signal over the range of analyte concentration relevant to the aimed application. The availability of miniaturized pumps and strategies to control flow along fluidic structures, some of which have been already incorporated in lab-on-chip demonstrators, make this objective amenable.

An open issue – also stemming from the use of the external optical components that has yet to be addressed is the compactness of the final system. Most interferometric sensors rely on coupling to external optical sources and detectors, which apart from sources of noise; add to the size of the final system. New approaches are required in terms of mechanical engineering to liberate the interferometric sensors from the laboratory optical tables and turn them into truly compact and moveable systems in order to be realistic solutions for PoN applications.

Finally, a significant drawback is the fact that so far interferometric sensors in most cases have been used as single-analyte devices. Few exceptions have demonstrated the feasibility of multi-analyte sensing (Ymeti et al., 2003; Misiakos et al., 2014a) within an interferometric detection scheme, and none has exceeded the simultaneous detection of two analytes. Despite the ability to integrate a large number of sensors on the same chip thanks to the well-established microfabrication technologies, there has yet to be a demonstration of real-time, multiplexed multi-analyte detection scheme. It seems that the restrictions for multi-analyte determinations are not set by the sensors performance per se but rather from the other system components such as the fluidics, the operation of the external optical and measurement set-up. Thus, it is not foreseen that integrated sensors can compete with the already available high throughout techniques in particular areas of applications such as molecular diagnostics or pharmaceutical studies. On the other hand, they could provide attractive solutions in areas where information on a limited number of analytes in a short time and with high accuracy is of paramount importance as in emergency clinical diagnostics or on-site environmental monitoring or food analysis. It is important to keep in mind that the pharmaceutical sector, which was very keen on supporting the development of label-free techniques, has become more reluctant since the mid-'00s to invest in them in light of the high throughput equipment already into use or commercially available (Cooper, 2006).

4.2.3. Future trends of interferometric sensors

The above-mentioned hurdles are not insurmountable; on the contrary, they should be seen as the challenges that need to be met and defeated sooner than later in the race of label-free PoN systems. Instead of struggling for the most sensitive interferometric sensor or the lowest LOD, most probably the new goal that needs to be set by the interferometric sensors is discovering the means to render them into truly-applicable, robust and reliable PoN systems. The future trend that should merge is first and foremost the extension of the existing sensors into multiplexed formats. Secondly, but equally important should be solutions ensuring system stability in a compact format which employs interrogation instrumentation allowing user-friendly operation. On the other hand, if the envisioned applications are such that requires the ultimate degree of sensitivity, most probably multi-wavelength interferometry is the key since it already has been proven capable of discriminating between specific binding and bulk refractive index changes. At the same time, surface chemistry must employ in order to expand the bio-functionalization techniques and the sample preparation, in such ways that interferometric sensing can be applied directly to complex media like blood, saliva, and food produce and products. Last but not least, fluid dynamics must be employed more intensively in order to develop real-life PoNs. Towards this direction, the interferometric sensors, through their ability to monitor reaction dynamics in real-time, may be applied as a powerful analytical tool to solve two problems at the same time: to get a more in-depth understanding of biomolecular interactions which in turn will help the research community develop the next generation of sensors for a wider range of real life applications. In summary, the advantages and disadvantages of the approaches presented in this review article are summarized in Table 3.

5. Conclusions

Microfabrication technologies have opened up a new pathway for label-free sensing, offering the opportunity for scalable fabrication and miniaturization of interferometric sensors that are promising candidates for a large variety of PoN applications. These versatile sensors offer high sensitivities and low LODs not easily attained by other optical techniques that either requires labeling or rely on pm-shift analysis. Their potential for high degree of integration and their subsequent utilization for real-time multi-analyte detection schemes add to them one more attractive attribute. Still, interferometric sensors have several technological challenges that need to be met and overcome in order to become the functional core of viable PoN systems.

Please cite this article as: Makarona, E., et al., Point-of-Need bioanalytics based on planar optical interferometry, Biotechnol Adv (2016), http://dx.doi.org/10.1016/j.biotechadv.2016.02.005

Table 3
Advantages of disadvantages of the various interferometric principles of operation.

	SW-MZI	BB-MZI	Monolithic BB-MZI	Bi-modal MZ	SW-YI	MW-YI
LOD	+	++	+[1]/++[2]	+	+++	+++
Need for external optical components/mechanical stability	−	+	+++[1]/+[2]	−	−	−
Size and cost of final system	−	+	+++/++	−	−	−
Signal ambiguities	−	+++	+++	++	−	++
Ease-of-data-analysis/user friendliness	+	−	−	−	+	−
Simultaneous determination of protein thickness and refractive index	−	−	+++	−	−	+++

[1] For the case of the fully-integrated BB-MZI as described in Misiakos et al. (2014b).
[2] For the case of the fully-integrated BB-MZI as described in Misiakos et al. (2014a).

No matter what the targeted application is, an interferometric sensor most probably exists or may be tailored and adapted to fulfill the PoN system specifications required for the envisioned application. It is certain that one would have to weigh the advantages and disadvantages of each interferometric scheme before the final choice, but it is also certain that interferometry is a powerful armory that can provide the best-fitted weapon to reach the specific target set. In that sense, interferometric sensors need not be developed in an antagonistic manner but rather in a synergistic one, since all routes have the potential to lead and be tailored to solutions that answer to specific applications. Prioritizing the three basic requirements of sensitivity (viewed as effective index of refraction LOD), accuracy (discrimination between specific, non-specific and bulk refractive index changes) and portability (including the issue of robustness, insensitivity to environmental changes and user-friendliness), one may have a ready-made guide to select the appropriate pathway towards solving one's own analytical problem at hand. Still, there is a lot that has to be done and several issues to be overcome, but it seems that the sky will be the limit for the next generation of interferometric sensors.

Acknowledgments

The authors would like to thank Mr. Alex Salapatas (INN, NCSR 'Demokritos') for the drawings of the article. This work was financially supported by the EU-FP7 funded Project "FOODSNIFFER" (FP7-ICT-318319), and the project "AURORA" funded by the Ministry of Education and Religious Affairs, GSRT - Management and Implementation Agency for RTD and Innovation Activities, O.P. Competitiveness and Entrepreneurship (EPAN II), contract no SYN11_5_1517.

References

Angelopoulou, M., Botsialas, A., Salapatas, A., Petrou, P.S., Haasnoot, W., Makarona, E., Jobst, G., Goustouridis, D., Siafaka-Kapadai, A., Raptis, I., Misiakos, K., Kakabakos, S.E., 2015. Assessment of goat milk adulteration with a label-free monolithically integrated optoelectronic biosensor. Anal. Bioanal. Chem. 407, 3995–4004.

Anopchenko, A., Marconi, A., Sgrignuoli, F., Cattoni, L., Tengattini, A., Pucker, G., Jestin, Y., Pavesi, L., 2013. Electroluminescent devices based on nanosilicon multilayer structures. Phys. Status Solidi A 210, 1525–1531.

Awsiuk, K., Bernasik, A., Kitsara, M., Budkowski, A., Petrou, P., Kakabakos, S., Prauzner-Bechcicki, S., Rysz, J., Raptis, I., 2012. Spectroscopic and microscopic characterization of biosensor surfaces with protein/amino-organosilane/silicon structure. Colloids Surf. B: Biointerfaces 90, 159–168.

Awsiuk, K., Budkowski, A., Petrou, P., Bernasik, A., Marzec, M.M., Kakabakos, S., Rysz, J., Raptis, I., 2013a. Model immunoassay on silicon surfaces: vertical and lateral nanostructure vs. protein coverage. Colloids Surf. B: Biointerfaces 103, 253–260.

Awsiuk, K., Budkowski, A., Psarouli, A., Petrou, P., Bernasik, A., Kakabakos, S., Rysz, J., Raptis, I., 2013b. Protein adsorption and covalent bonding to silicon nitride surfaces modified with organo-silanes: comparison using AFM, angle-resolved XPS and multivariate ToF-SIMS analysis. Colloids Surf. B: Biointerfaces 110, 217–224.

Banuls, M.-J., Puchades, R., Maquieira, A., 2013. Modifications development of silicon based label free integrated optical (IO) biosensors: a review. Anal. Chim. Acta 777, 1–16.

Blanco, F.J., Agirregabiria, M., Berganzo, J., Mayora, K., Elizalde, J., Calle, A., Dominguez, C., Lechuga, L.M., 2006. Microfluidic-optical integrated CMOS compatible devices for label-free biochemical sensing. J. Micromech. Microeng. 16, 1006–1016.

Brandenburg, A., 1997. Differential refractometry by an integrated-optical Young interferometer. Sensors Actuators B 38–39, 266–271.

Brandenburg, A., Henninger, R., 1994. Integrated optical Young interferometer. Appl. Opt. 25, 5941–5947.

Brandenburg, A., Krauter, R., Kunzel, C., Stefan, M., Schulte, H., 2000. Interferometric sensor for detection of surface-bound bioreactions. Appl. Opt. 34, 6396–6405.

Bras, M., Dugas, V., Bessueille, F., Cloarec, J.P., Martin, J.R., Cabrera, M., Chauvet, J.P., Souteyrand, E., Garrigues, M., 2004. Optimisation of a silicon/silicon dioxide substrate for a fluorescence DNA microarray. Biosens. Bioelectron. 20, 797–806.

Brosinger, F., Freimuth, H., Lacher, M., Ehrfeld, W., Gedig, E., Katerkamp, A., Spener, F., Cammann, K., 1997. A label-free affinity sensor with compensation of unspecific protein interaction by a highly sensitive integrated optical Mach–Zehnder interferometer on silicon. Sensors Actuators B 44, 350–355.

Bruck, R., Melnik, E., Muellner, P., Hainberger, R., Lämmerhofer, M., 2011. Integrated polymer-based Mach–Zehnder interferometer label-free streptavidin biosensor compatible with injection molding. Biosens. Bioelectron. 26, 3832–3837.

Brynda, E., Houska, M., Brandenburg, A., Wikerstal, A., 2002. Optical biosensors for real-time measurement of analytes in blood plasma. Biosens. Bioelectron. 17, 665–675.

Busse, S., Kashammer, J., Kramer, S., Mittler, S., 1999. Gold and thiol surface functionalized integrated optical Mach–Zehnder interferometer for sensing purposes. Sensors Actuators B 60, 148–154.

Caipa Campos, M.A., Paulusse, J.M.J., Zuilhof, H., 2010. Functional monolayers on oxide-free silicon surfaces via thiol–ene click chemistry. Chem. Commun. 46, 5512–5514.

Choo, S.J., Kim, J., Lee, K.Y., Ho Lee, D., Shin, H.-J., Ho, Park J., 2014. An integrated Mach–Zehnder interferometric biosensor with a silicon oxynitride waveguide by plasma-enhanced chemical vapor deposition. Curr. Appl. Phys. 14, 954–959.

Chynoweth, A., Mckay, K., 1956. Photon emission from avalanche breakdown in silicon. Phys. Rev. 102, 369–376.

Clark, L.C., Lyons, C., 1962. Electrode systems for continuous monitoring in cardiovascular surgery. Ann. N Y Acad. Sci. 102, 29–45.

Cooper, M.A., 2006. Optical biosensors: where next and how soon? Drug Discov. Today 11, 1061–1067.

Dante, S., Duval, D., Sepúlveda, B., González-Guerrero, A.B., Ramón Sendra, J., Lechuga, L.M., 2012. All-optical phase modulation for integrated interferometric biosensors. Opt. Express 20, 7195–7205.

Dante, S., Duval, D., Farina, D., Gonzalez-Guerrero, A., Lechuga, L.M., 2015. Linear readout of integrated interferometric biosensors using a periodic wavelength modulation. Laser Photonics Rev. 9, 248–255.

De Feijter, J.A., Benjamins, J., Veer, F.A., 1978. Ellipsometry as a tool to study the adsorption behavior of synthetic and biopolymers at the air–water interface. Biopolymers 17, 1759–1772.

Densmore, A., Xu, D.X., Janz, S., Waldron, P., Lapointe, J., Mischki, T., Lopinski, G., Delage, A., Schmid, J.H., Cheben, P., 2008. Sensitive label-free biomolecular detection using thin silicon waveguides. Adv. Opt. Technol. 725967.

Densmore, A., Vachon, M., Xu, D.X., Janz, S., Ma, R., Li, Y.H., Lopinski, G., Delâge, A., Lapointe, J., Luebbert, C.C., Liu, Q.Y., Cheben, P., Schmid, J.H., 2009. Silicon photonic wire biosensor array for multiplexed real-time and label-free molecular detection. Opt. Lett. 34, 3598–3600.

Dér, A., Valkai, S., Mathesz, A., Andó, I., Wolff, E.K., Ormos, P., 2010. Protein-based all-optical sensor device. Sensors Actuators B 151, 26–29.

Drapp, B., Piehler, J., Brecht, A., Gauglitz, G., Luff, B.J., Wilkinson, J.S., Ingenhoff, J., 1997. Integrated optical Mach–Zehnder interferometers as simazine immunoprobes. Sensors Actuators B 38–39, 277–282.

Duval, D., Gonzalez-Guerrero, A.B., Dante, S., Osmond, J., Monge, R., Fernandez, L.J., Zinoviev, K.E., Domınguez, C., Lechuga, L.M., 2012. Lab chip nanophotonic lab-on-a-chip platforms including novel bimodal interferometers, microfluidics and grating couplers. Lab Chip 12, 1987–1994.

Estevez, M.C., Alvarez, M., Lechuga, L.M., 2012. Integrated optical devices for lab-on-a-chip biosensing applications. Laser Photonics Rev. 6, 463–487.

Fan, X., White, I.M., 2011. Optofluidic microsystems for chemical and biological analysis. Nat. Photonics 5, 591–597.

Fan, X., White, I.M., Shopova, S.I., Zhu, H., Suter, J.D., Sun, Y., 2008. Sensitive optical biosensors for unlabeled targets: a review. Anal. Chim. Acta 620, 8–26.

Gao, Y., Gan, Q., Xin, Z., Cheng, X., Bartol, F.J., 2011. Plasmonic Mach–Zehnder interferometer for ultrasensitive on-chip biosensing. ACS Nano 5, 9836–9844.

Heideman, R.G., Lambeck, P.V., 1999. Remote opto-chemical sensing with extreme sensitivity: design, fabrication and performance of a pigtailed integrated optical phase-modulated Mach–Zehnder interferometer system. Sensors Actuators B 61, 100–127.

Heideman, R.G., Kooyman, R.P.H., Greve, J., 1991. Development of an optical waveguide interferometric immunosensor. Sensors Actuators B 4, 297–299.

Heideman, R.G., Kooyman, R.P.H., Greve, J., 1993. Performance of a highly sensitive optical waveguide Mach–Zehnder interferometer immunosensors. Sensors Actuators B 10, 209–217.

Please cite this article as: Makarona, E., et al., Point-of-Need bioanalytics based on planar optical interferometry, Biotechnol Adv (2016), http://dx.doi.org/10.1016/j.biotechadv.2016.02.005

Hiraoui, M., Guendouz, M., Lorrain, N., Haji, L., Oueslati, M., 2012. Buried anti resonant reflecting optical waveguide based on porous silicon material for an integrated Mach Zehnder structure. Appl. Phys. Lett. 101, 191114.
Hoffmann, C., Schmitt, K., Brandenburg, A., Hartmann, S., 2007. Rapid protein expression analysis with an interferometric biosensor for monitoring protein production. Anal. Bioanal. Chem. 387, 1921–1932.
Hong, J., Choi, J.S., Han, G., Kang, J.K., Kim, C.M., Kim, T.S., Sung, Yoon D., 2006. A Mach–Zehnder interferometer based on silicon oxides for biosensor applications. Anal. Chim. Acta 573–574, 97–103.
Hong, J., Yoon, D., Song, Kim T., 2009. The Mach–Zehnder interferometer based on silicon oxides for label free detection of C-reactive protein (CRP). Biochip J. 3, 1–11.
Jiang, X., Chen, Y., Yu, F., Tang, L., Li, M., He, J.J., 2014. High-sensitivity optical biosensor based on cascaded Mach–Zehnder interferometer and ring resonator using Vernier effect. Opt. Lett. 39, 6363–6366.
Kindt, J.T., Bailey, R.C., 2013. Biomolecular analysis with microring resonators: applications in multiplexed diagnostics and interaction screening. Curr. Opin. Chem. Biol. 17, 818–826.
Kitsara, M., Misiakos, M., Raptis, I., Makarona, E., 2010. Integrated optical frequency-resolved Mach–Zehnder interferometers for label-free affinity sensing. Opt. Express 18, 8193.
Koyun, A., Ahlatcıoğlu, E., Koca, İpek Y., 2012. Biosensors and Their Principles. In: Kara, S. (Ed.), A Roadmap of Biomedical Engineers and Milestones. ISBN: 978-953-51-0609-8 (Published: June 5).
Kozma, P., Hámori, A., Kurunczi, S., Cottier, K., Horvath, R., 2011. Grating coupled optical waveguide interferometer for label-free biosensing. Sensors Actuators B 155, 446–450.
Kozma, P., Kehl, F., Ehrentreich-Förster, E., Stamm, C., Bier, F.F., 2014. Integrated planar optical waveguide interferometer biosensors: a comparative review. Biosens. Bioelectron. 58, 287–307.
Langmuir, I., Shaefer, V.J., 1937. Optical measurement of the thickness of a film adsorbed from a solution. J. Am. Chem. Soc. 59, 1406.
Li, Y., Harris, E., Chen, L., Bao, X., 2010. Application of spectrum differential integration method in an in-line fiber Mach–Zehnder refractive index sensor. Opt. Express 18, 8135–8143.
Liu, Q., Tu, X., Woo Kim, K., Sheng Kee, J., Shin, Y., Han, K., Yoon, Y.-J., Lo, G.-Q., Kyoung, Park M., 2013. Highly sensitive Mach–Zehnder interferometer biosensor based on silicon nitride slot waveguide. Sensors Actuators B 188, 681–688.
Liu, Q., Woo Kim, K., Gu, Z., Sheng Kee, J., Kyoung, Park M., 2014. Single-channel Mach–Zehnder interferometric biochemical sensor based on two-lateral-mode spiral waveguide. Opt. Express 22, 27910–27920.
Liu, Q., Lim, S.Y., Soo, R.A., Park, M.K., Shin, Y., 2015. A rapid MZI-IDA sensor system for EGFR mutation testing in non-small cell lung cancer (NSCLC). Biosens. Bioelectron. 74, 865–871.
Lukosz, W., 1991. Principles and sensitivities of integrated optical and surface plasmon sensors for direct affinity sensing and immunosensing. Biosens. Bioelectron. 6, 215–225.
Lukosz, W., Tiefenthaler, K., 1983. Directional Switching in Planar Waveguides Effected by Adsorption–Desorption Processes. 2nd Eur Conf Integrated Optics (IEE conf), pp. 152–155.
Luo, D.H., Levy, R.A., Hor, Y.F., Federici, J.F., Pafchek, R.M., 2003. An integrated photonic sensor for in situ monitoring of hazardous organics. Sensors Actuators B 92, 121–126.
Ma, K., Ekblad, T., Klein Koerkamp, M., Kelderman, H., van Wijlen, M., Duarah, A., Yue, J., Zhang, L., Vee-Meng Wong, M., Hoo Lim, M., 2015. Contaminant detection in treated water using Optiqua's MiniLab biosensing system: a case study for Bisphenol A. Int. J. Environ. Anal. Chem. 95, 366–378.
Mach, L., 1892. Ueber einen interferenzrefraktor. Z. Instrumentenkd. 12, 89–93.
Markets and Markets survey, 2015. Biosensors Market by Application (Point of Care, Home Diagnostics, Research Labs, Biodefense, Environmental Monitoring, Food Industry), Product (Wearable, Non-Wearable), Technology (Electrochemical, Piezoelectric, Optical) & Geography - Analysis & Forecast to 2020.
Melnik, E., Bruck, R., Muellner, P., Hainberger, R., Lämmerhofer, M., 2011. Multi-step surface functionalization of polyimide based evanescent wave photonic biosensors and application for DNA hybridization by Mach–Zehnder interferometer. Anal. Chim. Acta 699, 206–2015.
Misiakos, K., Kakabakos, S.E., Petro, P.S., Ruf, H.H., 2004. A monolithic silicon optoelectronic transducer as a real-time affinity biosensor. Anal. Chem. 76, 1366–1373.
Misiakos, K., Raptis, Salapatas A., Makarona, E., Botsialas, A., Hoekman, M., Stoffer, R., Jobst, G., 2014a. Broad-band Mach–Zehnder interferometers as high performance refractive index sensors: theory and monolithic implementation. Opt. Express 22, 8856–8870.
Misiakos, K., Raptis, I., Makarona, E., Botsialas, A., Salapatas, A., Oikonomou, P., Psarouli, A., Petrou, P.S., Kakabakos, S.E., Tukkiniemi, K., Sopanen, M., Jobst, G., 2014b. All-silicon monolithic Mach–Zehnder interferometer as a refractive index and biochemical sensor. Opt. Express 22, 26803–26813.
Monat, C., Domachuk, P., Eggleton, B.J., 2007. Integrated optofluidics: a new river of light. Nat. Photonics 1, 106–114.
Mulder, H.K.P., Ymeti, A., Subramaniam, V., Kanger, J.S., 2012. Size-selective detection in integrated optical interferometric biosensors. Opt. Express 20, 20934–20950.
Nagel, T., Ehrentreich-Forster, E., Singh, M., Schmitt, K., Brandenburg, A., Berka, A., Bier, F.F., 2008. Direct detection of tuberculosis infection in blood-serum using three optical label-free approaches. Sensors Actuators B 129, 934–940.
Nassiopoulos, A.F., Grigoropoulos, S., Canham, L., Halimaoui, A., Berbezier, A., Gogolides, E., Papadimitriou, D., 1995a. Submicrometer luminescent porous silicon structures using lithographically patterned substrates. Thin Solid Films 255, 329–333.
Nassiopoulos, A.G., Grigoropoulos, S., Gogolides, E., Papadimitriou, D., 1995b. Visible luminescence from one-dimensional and 2-dimensional silicon structures produced by conventional lithographic and reactive ion etching techniques. Appl. Phys. Lett. 66, 1114–1116.
Nellen, P.M., Lukosz, W., 1993. Integrated optical input grating couplers as direct affinity sensors. Biosens. Bioelectron. 8, 129–147.
Piehler, J., Brecht, A., Geckeler, K.E., Gauglitz, G., 1996. Surface modification for direct immunoprobes. Biosens. Bioelectron. 11, 579–590.
Preechaburana, P., Gonzalez, M.C., Suska, A., Filippini, D., 2012. Surface plasmon resonance chemical sensing on cell phones. Angew. Chem. Int. Ed. 51, 11585–11588.
Prieto, F., Llobera, A., Jimenez, D., Domınguez, C., Calle, A., Lechuga, L.M., 2000. Analysis of silicon antiresonant reflecting optical waveguides for evanescent field sensors. J. Lightwave Technol. 18, 966–972.
Prieto, F., Sepulveda, B., Calle, A., Llobera, A., Domınguez, C., Lechuga, L.M., 2003. Integrated Mach–Zehnder interferometer based on ARROW structures for biosensor applications. Sensors Actuators B 92, 151–158.
Sarkar, D., Jamal, I., Mitra, S.K., 2013. Analysis design and fabrication of optical waveguides for Mach–Zehnder interferometry. Opt. Commun. 311, 338–345.
Sarkar, D., Siva Kumar Gunda, N., Jamal, I., SK, Mitra, 2014. Optical biosensors with an integrated Mach–Zehnder. Interferometer for detection of *Listeria monocytogenes*. Biomed. Microdevices 16, 509–520.
Schipper, E.F., Bergevoet, A.J.H., Kooyman, R.P.H., Greve, J., 1997a. New detection method for atrazine pesticides with the optical waveguide Mach–Zehnder immunosensors. Anal. Chim. Acta 341, 171–176.
Schipper, E.F., Brugman, A.M., Dominguez, C., Lechuga, L.M., Kooyman, R.P.H., Greve, J., 1997b. The realization of an integrated Mach–Zehnder waveguide immunosensor in silicon technology. Sensors Actuators B 40, 147–153.
Schlatter, D., Barner, R., Fattinger, C., Huber, W., Hiibscher, J., Hurst, J., Keller, H., Mangold, C., Miiller, F., 1993. The difference interferometer: application as a direct affinity sensor. Biosens. Bioelectron. 8, 109–116.
Schmitt, K., Schirmer, B., Hoffmann, C., Brandenburg, A., Meyrueis, P., 2007. Interferometric biosensor based on planar optical waveguide sensor chips for label-free detection of surface bound bioreactions. Biosens. Bioelectron. 22, 2591–2597.
Schneider, B.H., Edwards, J.G., Hartman, N.F., 1997. Hartman interferometer: versatile integrated optic sensor for label-free, real-time quantification of nucleic acids, proteins, and pathogens. Clin. Chem. 43, 1757–1763.
Schneider, B.H., Dickinson, E.L., Vach, M.D., Hoijer, J.V., Howard, L.V., 2000a. Highly sensitive optical chip immunoassays in human serum. Biosens. Bioelectron. 15, 13–22.
Schneider, B.H., Dickinson, E.L., Vach, M.D., Hoijer, J.V., Howard, L.V., 2000b. Optical chip immunoassay for hCG in human whole blood. Biosens. Bioelectron. 15, 597–604.
Schubert, T., Haase, N., Kuck, H., Gottfried-Gottfried, R., 1997. Refractive-index measurements using an integrated Mach–Zehnder interferometer. Sensors Actuators A 60, 108–112.
Sepulveda, B., Sanchez del Río, J., Moreno, M., Blanco, F.J., Mayora, K., Lechuga, L.M., 2006. Optical biosensor microsystems based on the integration of highly sensitive Mach-Zehnder interferometer devices. J. Opt. A: Pure Appl. Opt. 8, S561–S566.
Shew, B.Y., Cheng, Y.C., Tsai, Y.H., 2008. Monolithic SU-8 micro-interferometer for biochemical detections. Sensors Actuators A 141, 299–306.
Stamm, C., Dangel, R., Lukosz, W., 1998. Biosensing with the integrated-optical difference interferometer: dual wavelength operation. Opt. Commun. 153, 347–359.
Sun, Y.S., Landry, J.P., Fei, Y.Y., Zhu, X.D., Luo, J.T., Wang, X.B., Lam, K.S., 2008. Effect of fluorescently labeling protein probes on kinetics of protein–ligand reactions. Langmuir 24, 13399–13405.
Tiefenthaler, K., Lukosz, W., 1989. Sensitivity of grating couplers as integrated-optical chemical sensors. J. Opt. Soc. Am. B 6, 209–220.
Turner, A.P.F., 2000. Biosensors — sense and sensitivity. Science 290, 1315–1317.
Vroman, L., Adams, A.L., 1969. Findings with the recording ellipsometer suggesting rapid exchange of specific plasma proteins at liquid/solid interfaces. Surf. Sci. 16, 438–446.
Washburn, A.L., Bailey, R.C., 2011. Photonics-on-a-chip: recent advances in Integrated waveguides as enabling detection elements for real-world, lab-on-a-chip biosensing applications. Analyst 136, 227–236.
Weisser, M., Tovar, G., Mittler-Neher, S., Knoll, W., Brosinger, F., Freimuth, H., Lacher, M., Ehrfeld, W., 1999. Specific bio-recognition reactions observed with an integrated Mach–Zehnder interferometer. Biosens. Bioelectron. 14, 405–411.
White, I.M., Fan, X., 2008. On the performance quantification of resonant refractive index sensors. Opt. Express 16, 1020–1028.
Xu, J., Suarez, D., Gottfried, D.S., 2007. Detection of avian influenza virus using an interferometric biosensor. Anal. Bioanal. Chem. 389, 1193–1199.
Ymeti, A., Kanger, J.S., Greve, J., Lambeck, P.V., Wijn, R., Heideman, R.G., 2003. Realization of a multichannel integrated Young interferometer chemical sensor. Appl. Opt. 42, 5649–5660.
Ymeti, A., Kanger, J.S., Greve, J., Besselink, G.A.J., Lambeck, P.V., Wijn, R., Heideman, R.G., 2005. Integration of microfluidics with a four-channel integrated optical Young interferometer immunosensors. Biosens. Bioelectron. 20, 1417–1421.
Ymeti, A., Greve, J., Lambeck, P.V., Wink, T., van Hovell, S.W.F.M., Beumer, T.A.M., Wijn, R.R., Heideman, R.G., Subramaniam, V., JS, Kanger, 2007. Fast ultrasensitive virus detection using a Young interferometer sensor 7 pp. 394–397.
Young, T., 1802. The Bakerian lecture: on the theory of light and colours. Phil. Trans. R. Soc. London 92, 12–48.
Young, T., 1804. The Bakerian lecture: experiments and calculations relative to physical optics. Phil. Trans. R. Soc. London 94, 1–16.
Yu, H., Xiong, L., Chen, Z., Li, Q., Yi, X., Ding, Y., Wang, F., Lv, H., Ding, Y., 2014. Ultra compact and high sensitive refractive index sensor based on Mach–Zehnder interferometer. Opt. Lasers Eng. 56, 50–53.
Zehnder, L., 1891. Ein neuer interferenzrefraktor. Z. Instrumentenkd. 11, 275–285.
Zinoviev, K.E., González-Guerrero, A.B., Domínguez, C., Lechuga, L.M., 2011. Integrated bimodal waveguide interferometric biosensor for label-free analysis. J. Lightwave Technol. 29, 1926–1932.

Please cite this article as: Makarona, E., et al., Point-of-Need bioanalytics based on planar optical interferometry, Biotechnol Adv (2016), http://dx.doi.org/10.1016/j.biotechadv.2016.02.005